The Use of Graphene and its Derivatives in Chemical and Biological Sensing

By

Gregory Morgan

B. S. in Chemistry, Slippery Rock University, 2010

Submitted to the Graduate Faculty of

The Kenneth P. Dietrich School of Arts and Sciences

in partial fulfillment

of the requirement for the degree of

Master of Science

UNIVERSITY OF PITTSBURGH

2016

University of Pittsburgh

Kenneth P. Dietrich School of Arts and Sciences

This thesis was presented

by

Gregory Joseph Morgan

It was defended on

October 29, 2015

and approved by

Dr. Jill Millstone, Assistant Professor, Chemistry

Dr. Nat Rosi, Professor, Chemistry

Committee Chair: Dr. Alex Star, Professor, Chemistry

The Use of Graphene and its Derivatives in Chemical and Biological Sensing

Gregory Joseph Morgan, M.S.

University of Pittsburgh, 2016

Abstract

A chemical sensor is defined as a transducer comprised of, or coated with, a layer that responds to changes in its local chemical environment. Chemical sensors convert various forms of energy into a measurable signal. For instance, the chemical energy involved with bonds breaking or forming can change the electronic properties of the transducer, creating an observable signal such as an increase or decrease in electrical resistance. Chemical sensing is important in many facets of research including environmental, bio-medical/pharmaceutical, industrial, automotive, and human safety. For a sensor to be practical it must interact preferentially with the target chemical analyte. A sensor should be precise, accurate, robust, cost efficient to manufacture, low in power consumption, portable otherwise the sensor is undesirable. Another key value of chemical sensors is it must exhibit rapid detection. Prior to portable sensors chemical analysis was performed in a laboratory on large, expensive instruments, which is costly in time, equipment fees, and personnel wages to operate. These sophisticated instruments are accurate and precise, however, it is far more beneficial to have a miniature, on-site detection apparatus. The first environmental, on-site sensor was used by the mining industry to monitor subterranean air quality; the canary. Carbon monoxide and methane (colorless, odorless gases) are large

problems in the mining industry; smaller life forms are more susceptible to being poisoned by toxic gases. Today sensor constructs are far different from that of a canary, however, they serve the same purpose. Carbon nanomaterials such as graphene and single-walled carbon nanotubes and other derivatives prove to be of great importance in sensor research due to their unique electronic properties, and they're high aspect ratio allowing them to be highly sensitive to small perturbations in local electronic environments.

Table of Contents

List of Figures

1.0 Introduction

1.1 Sensors

A sensor has a specifically functioning transducer. A transducer is a component that converts one type of energy (input) into another (output). Transducers are common elements in everyday life such as the antenna on a radio converting electromagnetic waves into electrical signals which are subsequently converted into sound waves by a transducer in the radio's speaker. Light bulbs convert electrical current into photons. Many other transducers exist: electrochemical, electromechanical, electroacoustic, electro-optical, thermoelectrical, and radioacoustic. A sensor is a device consisting of a transducer that detects a specified change in its environment. There are two general types of sensors: contact and non-contact. Contact sensors are devices that require physical contact of analyte or force to produce an output such as chemical sensors and mechanical/pressure sensors. Non-contact sensors produce outputs in the presence of a non-physical energy such as a magnetic or electric field. Herein we will look at contact sensors utilizing carbon nanomaterial-based transducers, specifically graphene and its derivatives. We will discuss the synthesis and characterization of these materials, the electronic properties, and the applications in chemical and biological sensors.

1.1.1 Chemical Sensors

A chemical sensor is defined as a transducer comprised of, or coated with, a layer that responds to changes in its local chemical environment.[1] Chemical sensors convert various forms of energy into a measurable signal. For instance, the chemical energy involved with bonds breaking or forming can change the electronic properties of the transducer, creating an observable signal such as an increase or decrease in electrical resistance. Chemical sensing is important in many

facets of research including environmental, bio-medical/pharmaceutical, industrial, automotive, and human safety. For a sensor to be practical it must interact preferentially with the target chemical analyte. Other important aspects of sensor research are to make devices that are precise, accurate, robust, be cost efficient to manufacture, and have low energy consumption, otherwise the sensor is undesirable. Another key value of chemical sensors is to be portable and also, must exhibit rapid detection. Prior to portable sensors chemical analysis was performed in a laboratory on large, expensive instruments, which is costly in time, equipment fees, and personnel wages to operate. These sophisticated instruments are accurate and precise, however, it is far more beneficial to have a miniature, on-site detection apparatus. The first environmental, on-site sensor was used by the mining industry to monitor subterranean air quality; the canary. Carbon monoxide and methane (colorless, odorless gases) are large problems in the mining industry; fortunately for the miners of old, smaller life forms are more susceptible to being poisoned by these gases. Today sensor constructs are far different from that of a canary, however, they serve the same purpose.

1.1.1.1 Field-Effect Transistors

Two common types of electrical transducers are field-effect transistors (FET) and chemiresistors. The field of FETs has grown since their introduction in the 1970s. A field-effect transistor is a three electrode device consisting of a source and drain electrode bridged by a semiconducting material, typically silicon, and a gate electrode. A voltage bias is held across the source and drain electrodes, and the gate electrode acts as an on/off switch. Semiconductors “turn on” and pass current when acted upon by a particular electric field emitted by the gate electrode, and likewise, “turn off” by becoming highly resistive and halt the passage of current. There are two types of FETS, back gated, or liquid gated, depicted in Figure 1 with a carbon nanotube as the

semiconductor. Back gated FETs are fabricated in such a way that the substrate (a conductor) is coated with an insulator, then patterned with electrodes. The conducting substrate is then connected to act as the gate electrode. Liquid gating is fabricated so that the source and drain electrodes are patterned on an insulating substrate and the device is submerged in solution into which the gate electrode is also submerged.[2]

1.1.1.2 Chemiresistors

The other sensor construct commonly utilized is the chemiresistor, a variable resistor that changes in resistance in response to is local chemical environment.[3] Chemiresistors consist of a source and drain electrode bridged with a semiconducting material (Figure 1). This design is simpler than the FET due to the lack of gate electrode.

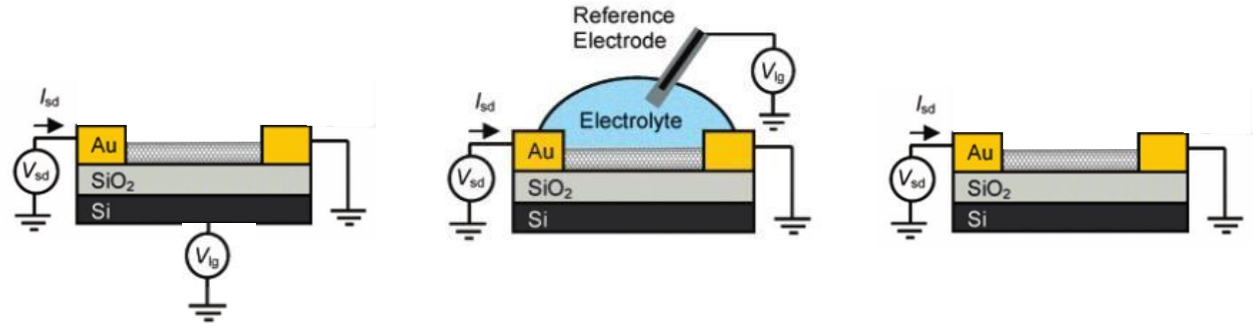

Figure 1: Diagrams of a back gated and liquid gated FETs, and a chemiresistor. Adapted from reference 2, with permission American Chemical Society, Copyright 2008.

1.2 Carbon Nanomaterials

By definition a nanomaterial must have at least one dimension between 1-100 nm. Due to their remarkable chemical properties carbon nanomaterials have been the focus of vast amounts of research for chemical sensing. Carbon exists in several forms, each with different chemical and physical properties, depending on its chemical bond nature. When in the sp^3, tetrahedral

configuration carbon exists as the diamond, one of nature's strongest minerals. It also exhibits several sp^2 hybridized allotropes where graphene, an atomic layer of carbon, is the mother of all other sp^2 forms (Figure 2).[4] Graphene can be wrapped together forming a single layered sphere, the 0-dimensional Buckminsterfullerene,[5] it can be rolled into a cylinders creating the 1-

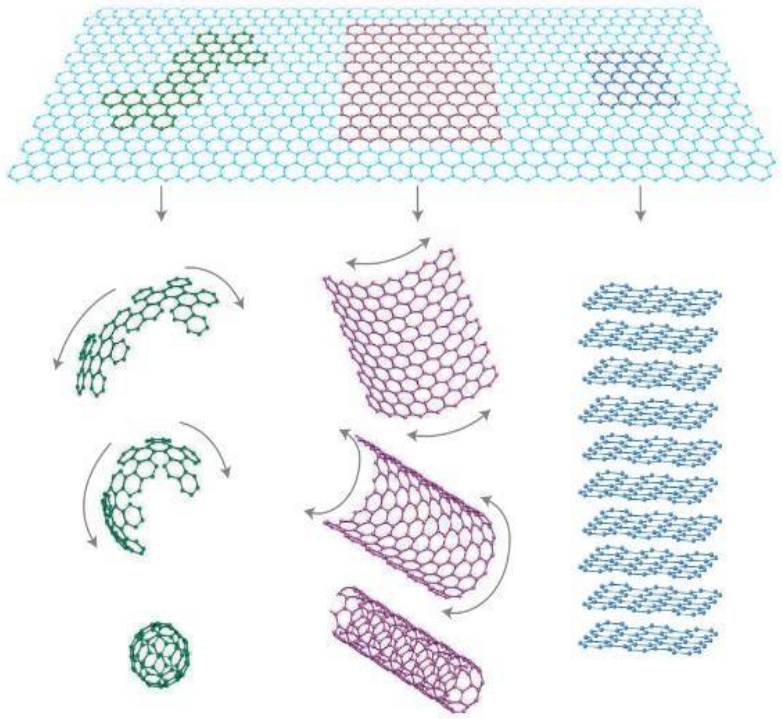

Figure 2: The basis of all graphitic forms, graphene (top), can be wrapped into fullerenes, rolled into nanotubes, or stacked into graphite. Adapted from reference 4 with permission from Nature Publishing Group, copyright 2007.

dimensional single-walled carbon nanotube (SWNT), multiple concentric cylinders form multi-walled nanotubes, and lastly, stacking layers of graphene creates 3-dimensional graphite. SWNTs have been of great interest for research due to their incredible strength, and their metallic and semiconducting electronic properties. For instance, single-walled carbon nanotubes have been proposed for the space elevator due to their light weight, and stronger than steel strength. Their electronic properties make them a target for chemical sensors research.

2.0 Characterization Methods of Nanomaterials

2.1 Microscopy

By definition, nanomaterials must have at least one dimension in the size range 1 to 100 nm and therefore, require highly sophisticated instruments to achieve this nanoscale resolution. There are many types of optical microscopes that originated with hand held magnifying lenses. However, like the hand-held lens, many of these microscopes use light as the probe. These are good for viewing macro- and microscopic objects such as plant and animal cells, even bacterial specimens, but still lack the resolution to visualize objects in the nanoscale because the resolution is within the order of the wavelength of light being used (visible light ~400-750 nm). To image such small matter we must utilize more advanced techniques using probes such as electrons and atomically fine tips.

2.1.1 Transmission Electron Microscopy

The transmission electron microscope (TEM) was developed nearly a century ago with experiments following cathode ray tubes and the ability to change the trajectory of electrons, in a vacuum, using magnetic fields. Using electrons as the probe enables the user to observe much finer details of structures. The TEM functions much like an optical microscope only in place of physical glass lenses to refract light it uses electromagnets to refract electrons. The TEM has few sample requirements, it must be able to exist in a vacuum and also must be thin enough for electrons to pass through it completely. Electrons emitted from a filament are accelerated through a series of electromagnetic lenses (80-100 keV), pass through the sample, and are then refocused and projected onto either a phosphor screen below or into a charge-coupled device

(CCD) camera. As the electrons pass through the sample they are deflected by materials present on the TEM grid and appear darker in the image. Samples that are too thick turn up black and indiscernible if the electron beam cannot pass through. This is a great method for looking at nanomaterials, more so with a high resolution TEM (HRTEM) which can actually see and measure crystal lattice lines and spacing, and in some cases reach atomic resolution.

2.1.2 Scanning Electron Microscopy

Scanning electron microscope (SEM) is a technique used to look at the external morphology of a sample, much like an optical microscope, however, the resolution of SEM is much higher because it also uses electrons as the probe. Electrons are accelerated toward the sample surface at which several situations could occur. The electron could elastically reflect back off of the surface or penetrate the surface and eventually leave the surface again as backscattered electrons. The impinging electrons might also inelastically penetrate the surface, excite the sample, and release either secondary electrons, Auger electrons, or X-rays. Most electrons penetrate the surface and shortly after are reflected as back scattered electrons where they are collected by a detector and analyzed or resolved into an image through a computer.

2.1.3 Scanning Tunneling Electron Microscopy

Scanning tunneling electron microscopy is a technique which allows atomic resolution of conductive surfaces. A bias voltage is held across a metallic tip and a conductive surface, as the two are brought to within one nanometer of each other, a measurable current is detected as electrons tunnel across the substrate-tip gap.[6] It has been used to view individual molecules on substrates and even single atoms of substrate materials.

2.1.4 Atomic Force Microscopy

Atomic force microscopy is a method of imaging surfaces with atomic resolution by bringing a probe into close proximity and sensing the interactions with the surface while rastering over a defined area.[7] In atomic force microscopy a cantilever oscillates at a particular frequency. As the cantilever is brought close to a surface, a sharp tip interacts with the surface atoms. Changes in the height profile of the surface change the amplitude of oscillation which is then recorded via a reflected laser and converted to an image of the surface. This method is very high resolution, able to detect height differences under 1 nm.

2.2 Spectroscopy

2.2.1 Raman Spectroscopy

Raman spectroscopy is a widely utilized, nondestructive method of characterizing carbon nanotubes and graphene species. Typical Raman spectra of pristine nanotubes or graphene show a distinct peak at 1580 cm^{-1}, this corresponds to a primary in-plane vibrational mode exhibited by

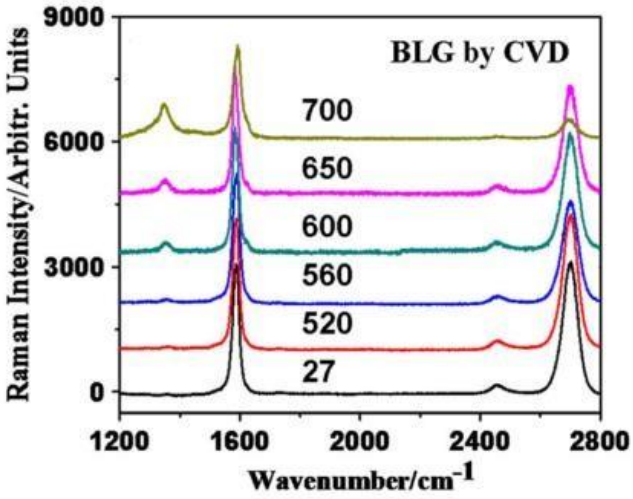

Figure 3: Raman spectra of bilayer graphene to different temperatures in air. Adapted from reference 9 with permission from Wiley, copyright 2013.

sp^2 carbon lattices. Other characteristic peaks are the D and its second-order overtone 2D peak. The 2D is present in pristine graphite and graphene sheets, whereas the D appears in the spectrum as a result of an inelastic scattering by phonons in the lattice, i.e. defect sites such as oxidation sites or intercalated heteroatoms in the lattice. The D peak disappears for perfect crystals.[8] Figure 3 displays Raman spectra with increasing D bands as samples of bilayer graphene are heated in air to increasing temperatures.[9]

2.2.2 X-ray Photoelectron Spectroscopy

A Swedish physicist by the name of Kai Siegbahn was awarded the Nobel Prize in the 80's for his work on what he called electron spectroscopy for chemical analysis (ESCA). ESCA, also known as X-ray photoelectron spectroscopy (XPS), impinges a sample with x-rays of a particular energy and measures the kinetic energy (E_k) of ejected electrons. The kinetic energy is related to the binding energy (E_b) of the electron through the equation

$$E_b = hv - E_k - w$$

where w is the spectrometers work function, correcting for the electrostatic environment in which the electron is produced and measured, h is Planck's constant (6.626×10^{-34}Js), and v is the frequency of the impinging photon. Binding energies are unique to atomic and molecular orbitals which allow XPS to identify atomic composition and the oxidation state of the atoms present. Figure 4 shows typical survey and high resolution carbon spectra collected by XPS.

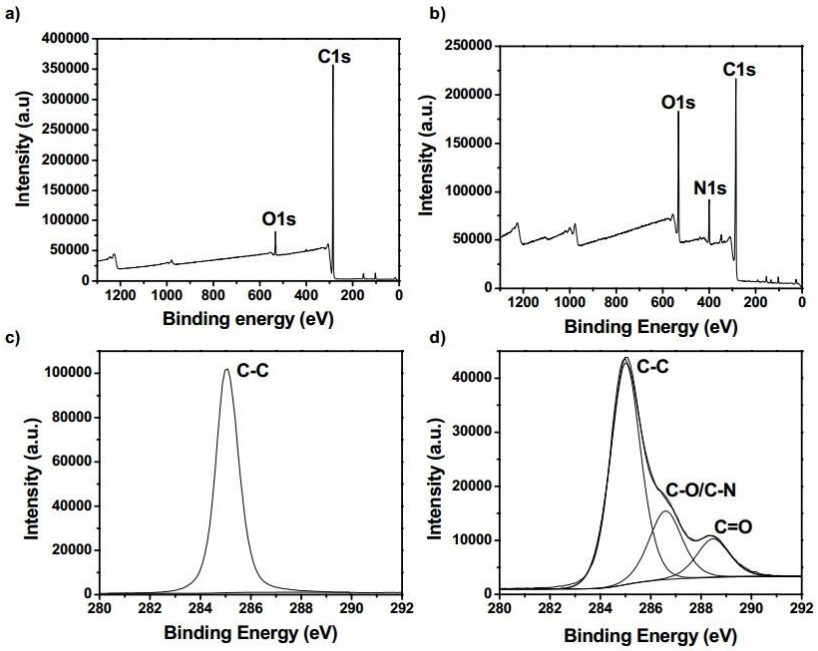

Figure 4: XPS spectra of reduced graphene oxide (RGO) and holey reduced graphene oxide (hRGO). Survey scans of a) RGO and b) hRGO. High-res C1s scans of c) RGO and d) hRGO. RGO contains a total of 4.32 atomic% O, while hRGO contains 25.2 atomic % O. hRGO also contains 10. 5% N as a result of the binding of NH_4^+ or hydrazine to carboxylic acid groups which was not fully removed by dialysis. Adapted from reference 30 with permission from the American Chemical Society, copyright 2014.

3.0 Carbon Nanotubes

Carbon nanotubes have different electronic properties varying with the symmetry of the carbon nanotube along its longitudinal axis. Carbon nanotubes are conveniently visualized as a roll-up of a rectangular graphene sheet so each atom of two opposing edges meet to form a cylinder. Due to the hexagonal lattice there are two structures that can occur, named for the arrangement of the carbon atoms at the open ends of the nanotube: zig-zag and armchair (Figure 5). Within these configurations nanotubes are identified by two fundamental vector numbers (*n* and *m*) which define the two carbon atoms of a sheet of graphene that are bonded together to form its circumference.[10] If *n* is an integer and *m*=0, the nanotube will take on a zig-zag confirmation. However, when *n* and *m* are equal the nanotube is in the armchair confirmation. Any combination of numbers in between results in a chiral nanotube. Chirality is an asymmetric property in which a molecule has a non-superimposable mirror image of itself, much like

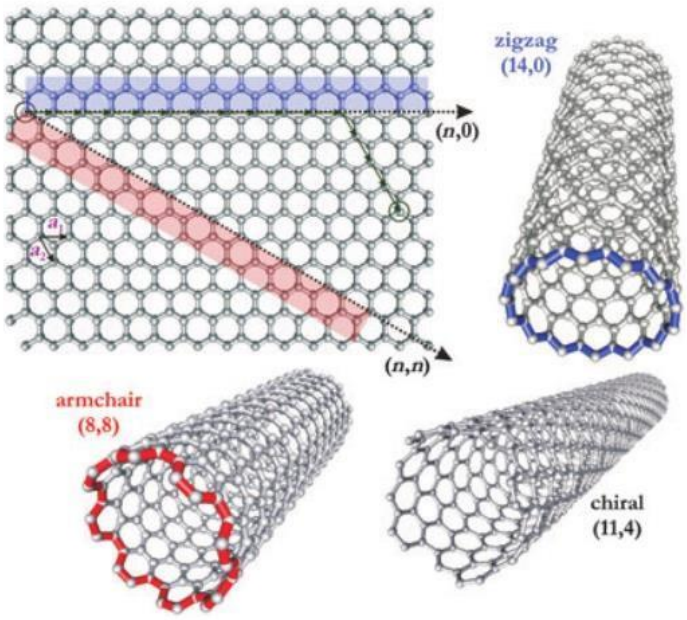

Figure 5: Roll-up of graphene sheet leading to the three different types of SWNTs. Adapted from reference 10 with permission from Wiley, copyright 2005.

humans have a right and left hand. Nanotubes can be either metallic or semiconducting depending on their chirality. If the vectors $m - n = 3x$ (where x is an integer) the nanotube will be metallic in nature. Metallic nanotubes account for one third of all nanotubes and include all armchair tubes.

Metallic nanotubes have zero band gap (0.0 eV), whereas, semiconducting carbon nanotubes do exhibit a band gap (0.4-0.7 eV depending on tube diameter). Thus, semiconducting nanotubes are ideal for use in place of silicon in FET sensors. Also, due to their structure, every atom is on the tube's surface making them highly susceptible to the smallest electrical perturbations. There has been extensive research done on 1-D carbon nanomaterials to date.[11-14] Carbon nanotubes have been utilized as the base material for the detection of pH,[3] biological markers,[15, 16] biological interactions,[17-20] various gasses,[1, 21-26] metal ions,[27] and reactive oxygen species.[28] Carbon nanotubes can be functionalized to make them more sensitive and selective to a particular analyte. This can be done by covalent or non-covalent functionalization. Covalent functionalization to a pristine carbon nanotube can be done through electrochemical modifications with molecules such as diazonium ions.[29] Partially oxidized carbon nanotubes may also be functionalized through chemical methods such as 1-ethyl-3-(3-dimethylaminopropyl)-carbodiimide (EDC) and n-hydroxysuccinimide (NHS).[30] EDC/NHS chemistry binds primary amines, found in molecules, proteins, and aminoacids, to carboxylic acids on the oxidized nanotubes. This covalent binding to the nanotube decreases the aromaticity by introducing sp^3 carbon sites which also creates electron scattering sites, lessening the conductance.

3.1 Synthesis

Current methods of carbon nanotube synthesis include electric arc-discharge, laser ablation of

graphite, or chemical vapor deposition.[10] Electric arc-discharge is a process where a high current (~100 A) is passed through high purity graphite electrodes (~6 mm diameter) spaced 1-2 mm apart, in a helium atmosphere (500 torr).[31] Multiwalled nanotubes and fullerenes are collected on the cathode during arc-discharge, however, to create single walled nanotubes, the core of the electrode is bored out and filled with pure powered metals (Fe, Ni, and Co) and graphite. Downsides to this process are expensive graphite electrodes and non-desired byproducts such as fullerenes, carbon coated metal catalysts, and amorphous carbon. Finally, this process is not optimal for controlling the diameter of the nanotubes.

Laser ablation (or vaporization) is another method of multi-walled nanotube production which involves pulsing a high intensity laser onto a graphite source, located in a 1200 °C furnace, causing extreme localized heating (>3000 K) evaporating the carbon which is then carried by flowing argon to a water cooled collector (Figure 6).[32] Again, to obtain single-walled nanotubes metal catalysts must be incorporated into the target. However, this method is low yield and therefore costly for large scale production.

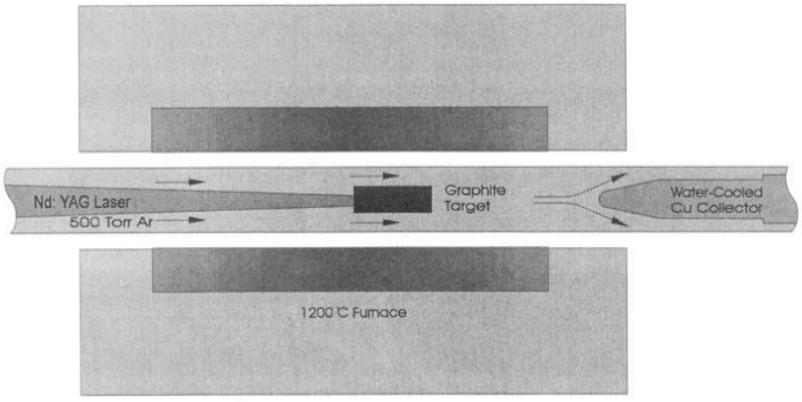

Figure 6: Schematic of the over laser-vaporization apparatus in which nanotubes were prepared. Adapted from reference 32 with permission from the American Chemical Society, Copyright 1995.

The most effective large scale production of nanotubes comes from chemical vapor

deposition (CVD).[33] This is a process where metal catalyst particles are prepared on a substrate via metal oxide calcination and a carbon source (hydrocarbon gas or vapor) is flown over the substrate, in a tube furnace at high temperature (900°C). The hydrocarbons are reduced on the surface of the metal catalysts to grow carbon nanotubes roughly the diameter of the catalyst particles.

4.0 Graphene

4.1 Synthesis

Due to its interesting electrical properties, researchers are continually searching for simpler, more efficient, and cost effective, or novel method of synthesizing graphene. To date, many methods have been identified and optimized to produce larger, more uniform, single crystalline sheets of graphene. As time progresses scientists are optimizing ways to control the number of layers during synthesis, minimizing grain boundaries, large area growth of graphene, and improving large scale transferring methods.

4.1.1 Mechanical Exfoliation

The most common example of mechanical exfoliation is the everyday use of a pencil in which graphite is pressed against paper, leaving behind thin layers of graphite. The first time single layer graphene was produced and described by Geim and Novoselov in 2004, is known as the scotch tape method.[34] Starting with graphite flakes they etched micron sized holes into the surface which they subsequently adhered to a photoresist coated silicon wafer. They then used commercial adhesive tape to lift away the graphene layers from the wafer. Through wet ball milling it is possible to achieve few-layer and even single-layer graphene.[35] This is, essentially, placing graphite flakes or powder into a tumbling chamber with water and steel spheres, which pulverize and separate layers due to impact and shear forces.

4.1.2 Hummers Method/Reduction of Graphene Oxide

One chemical procedure to produce graphitic oxide is the Hummers method[36] then exfoliate it into graphene oxide. Modifications have been made to the original procedure since its publication in the 1950's[37] and is used widely in the literature. Briefly, graphite flakes and

sodium nitrate are stirred in sulfuric acid. This solution is cooled to 0° C in an ice bath, then potassium permanganate is added slowly to ensure the temperature does not rise above 20° C. The solution is then heated to 35° C for 30 minutes before being diluted with water. It is then heated to 98° C for 15 minutes. The reaction solution is then diluted further and treated with hydrogen peroxide. While the solution is still warm, it is filtered and rinsed with excess water. The remaining solid is then sonicated to exfoliate graphene oxide sheets, and dialyzed to remove excess ions from the product. The final product is (ideally) single layer graphene oxide sheets. Graphene oxide, however, is an electrical insulator due to the high density of defect sites in the carbon lattice. This can be resolved by deoxygenation of the graphene oxide via thermal, mechanical, and chemical reductions.

One common pathway for the chemical deoxygenation of graphene oxide is liquid phase hydrazine hydrate reduction, recorded by Stankovich.[38] Exfoliated graphene oxide is suspended in water and refluxed at 100°C in an oil bath for 24 hours. The reduced graphene oxide precipitates out as a black solid which is filtered, washed with excess water followed by methanol, and dried. Reduction can also be done thermally by heating the graphene oxide in a tube furnace under an argon or argon/hydrogen atmosphere at high temperature.

4.1.3 Chemical Vapor Deposition

Chemical vapor deposition is a process in which a carbon precursor is passed through a high temperature furnace by a carrier gas and deposited onto a substrate that is either itself catalytic, or a support for passing catalysts. The precursor reacts with the catalyst to form sp^2 hybridized carbon lattices: graphene sheets on catalytic substrates or nanotubes stemming from nanoparticle catalysts. This method is also used to incorporate other hetero-atom functionalities such as nitrogen species by including an amine precursor.

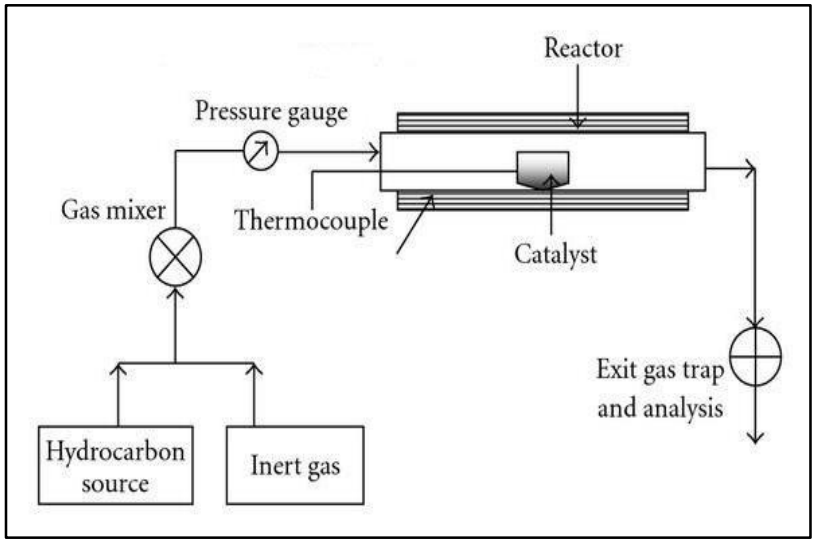

Figure 7: Schematic diagram of a CVD process for CNT synthesis. Reprinted with permission from the Hindawi, copyright 2010 (http://www.hindawi.com/journals/jnm/2010/395191/).

4.2 Electronic Properties of Graphene/Graphene Oxide

The electronic properties of graphene and its derivatives are typically analyzed in the form of current versus source-drain voltage, and many times tested as a field-effect transistor. Graphene field-effect transistor devices exhibit conductance in both the positive and negative voltage regions due to graphene's metallic nature.[39] This corresponds to the symmetric conductivity versus gate voltage curve (Figure 8). Carbon nanotubes, in most cases, are semiconducting due to quantum confinement caused by their diameter, however, some exhibit metallic properties due to the chirality of their structure (2:1 semiconducting: metallic). Carbon nanotubes have been extensively utilized as research targets in efforts to make smaller, bendable or wearable electronics, and even transparent electronics.[40, 41] This is also true for graphene.[42] Several

challenges must be overcome if a device made of graphene is to behave similarly to an analogous carbon nanotube device.

A carbon nanotube device would always be more sensitive to molecular analytes due to their 1-dimentional structure. The impinging analyte is typically on the size order of the nanotube which gives greater impact on the mobile charges in the system, whereas graphene sheets have a surface area much larger than individual molecules.[43, 44] The band structure of graphite was proposed by Wallace in 1947.[45] The valence and conduction bands meet at the Dirac point, hence zero bandgap. For a transistor based sensor this must be overcome to enable graphene to act as a semiconductor. This is why for carbon based nano-electronics and sensing capabilities you must limit the width of travel and the number of energy barriers the charge carriers must pass.

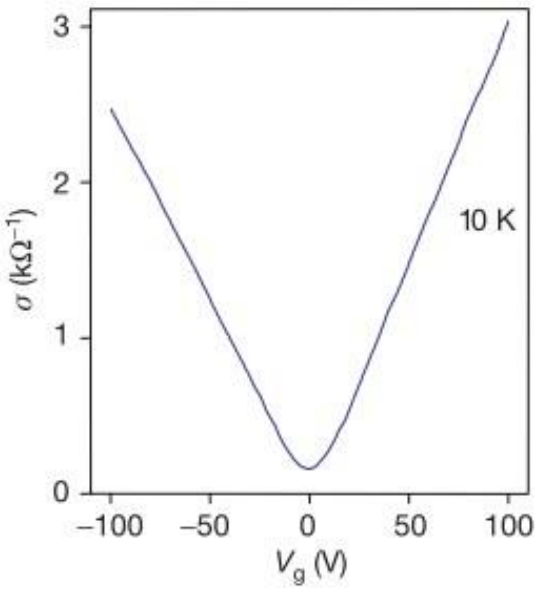

Figure 8: Changes in graphene's conductivity (σ). Adapted from reference 39 with permission from Nature Publishing Group, copyright 2005.

4.3 Sensor Applications of Graphene

Much work has been recorded using graphene as a sensor transducer to detect CO_2[46], pH[47], other gases, and vapors. Graphene is also used as a coating of fibers[48] and quartz crystal microbalances[49] for the detection of volatile organic compounds. However, many of these sensors require high temperatures in order for larger responses; high temperature means high energy and higher cost of functionality. This can be alleviated by functionalizing the graphene to respond more specifically to particular analytes at lower, ambient temperatures.

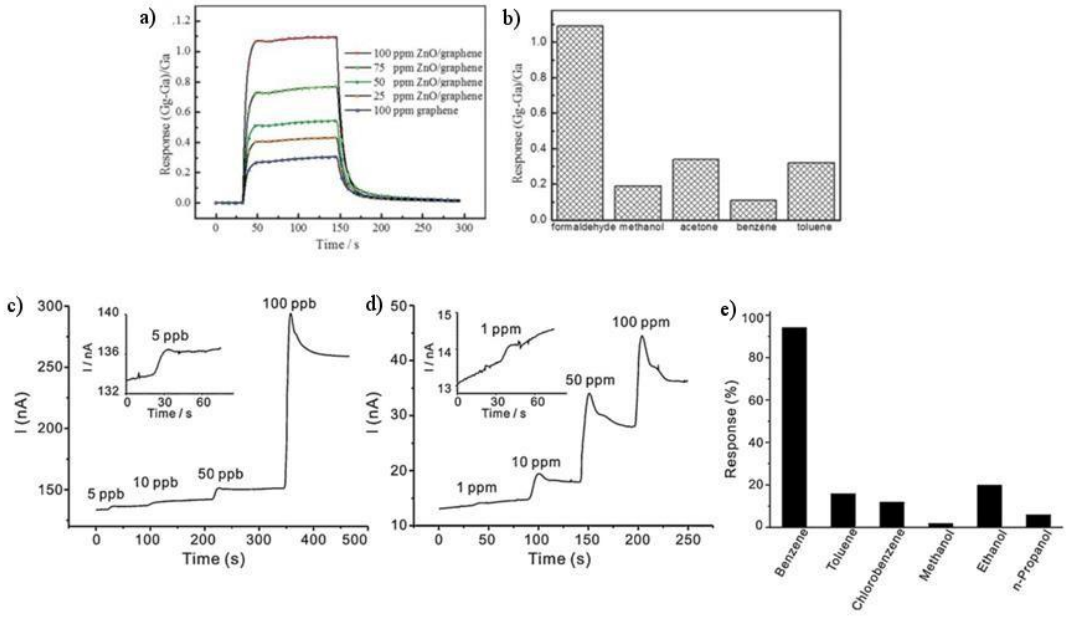

Figure 9: (a) The response curve of ZnO QDs/graphene sensors and pure graphene sensors to the formaldehyde gas at different concentrations; **(b)** the response of ZnO QDs/graphene sensors to several gases at the concentration of 100 ppm. Adapted from reference 50 with permission from the Royal Society of Chemistry, copyright 2012. Response curves of **(c)** the SnO_2/graphene nanocomposite and **(d)** the traditional SnO_2 to benzene. **(e)** Comparison of the responses of the SnO_2/graphene nanocomposite to 100 ppb of different VOCs. Adapted from reference 51 with permission from Elsevier, copyright 2012.

Graphene has been functionalized with metal oxide nanoparticles such as the work published by Huang et al.[50] using zinc oxide quantum dots to enhance the sensitivity to formaldehyde over other volatile organic chemicals (Figure 9 a,b). Meng et al. utilized 4-5 nm nanocrystals of tin oxide to detect parts per billion (ppb) levels of benzene.[51] Pairing the tin oxide nanoparticles with graphene sheets enhanced the signal so significantly that the hybrid sensor response to 100 ppb was greater than plane tin oxide's response to 100 parts per million (ppm) benzene (Figure 9 c,d). Figure 9e shows a comparison of responses to other organic molecules.

Aluminum oxide quantum dots were paired with graphene to make a CO_2 sensitive chemiresistor by Nemade and Waghuley.[52] The aluminum oxide quantum dots were synthesized through a sol-gel process and sintered at 500°C for 3 hours. They were then mixed varying the weight percent of graphene to create composites (20 – 80% graphene to 1 gram aluminum oxide). They tested these composites for sensitivity to CO_2 in humidity controlled air at room temperature and found the 80 wt% graphene Al_2O_3 composite had the greatest response and selectivity over liquid petroleum gas.

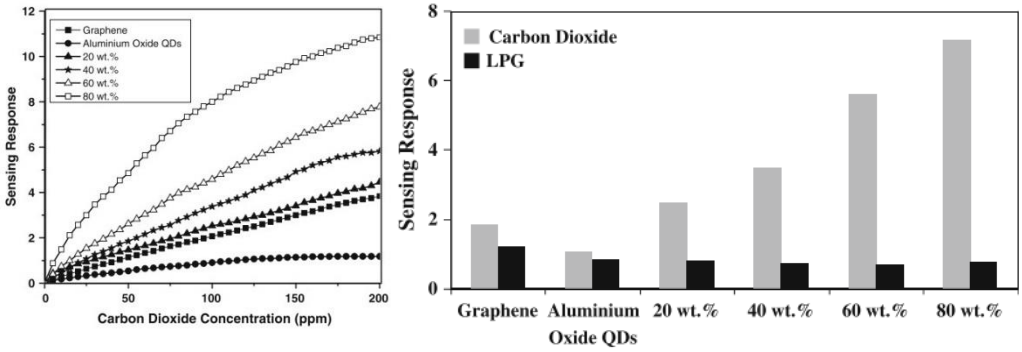

Figure 10: (Left) Variation of response of chemiresistors with the concentration of CO_2 at room temperature. (Right) Comparative gas sensing responses of chemiresistors towards CO_2 and liquid petroleum gas (LPG) for 40 ppm at room temp. Adapted from reference 52 with permission from Springer, copyright 2014.

Ammonia detection is highly important to monitor in environmental, automotive, chemical, and medical diagnostics fields.[53] Tannic acid functionalized-reduced graphene oxide has shown to be not only sensitive but highly selective to ammonia detection (Figure 11 a,b).[54] Yoo et al. describe a tannic acid functionalized reduced graphene oxide hybrid allowing room temperature detection of ammonia and claim mechanism enhancement through hydrogen bonding of the analyte to the targeting molecule. Another method of ammonia sensing is examined by Yang and coworkers, through which a porous, conductive polymer, poly(3,4-ethylenedioxythiophen) (PEDOT), was conjugated with reduced graphene oxide.[55] When rapidly dried, PEDOT forms a porous coating. It was discovered that changing the rate of temperature ramping changes the morphology of the PEDOT and likewise, the sensitivity to ammonia. The porous PEDOT/reduced graphene oxide was able to detect ammonia in the parts per billion range (Figure 11c).

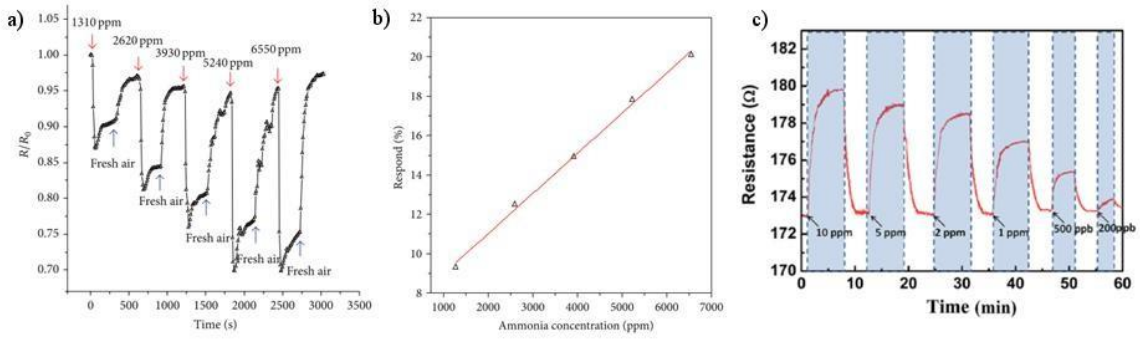

Figure 11: (a) Response of tannic acid functionalized reduced graphene oxide to NH_3, (b) linear response with increasing NH_3 concentration. Adapted from reference 54 with permission from Hindawi, copyright 2014. (c) Sensitivity of porous PEDOT/RGO based sensor to concentration NH_3 gas. Adapted from reference 55 with permission from the Royal Society of Chemistry, copyright

5.0 Graphene Nanoribbons

5.1 Synthesis

5.1.1 Lithographic Methods

It has been found that graphene nanoribbons act like nanotubes when comparable in width[56], therefore, much research has gone into creating them. A common production method is photo or electron-beam lithography. Briefly, lithography is a top down method of patterning structures onto a desired substrate be it electrodes on silicon wafers, holes in graphene, or nanoribbons. For nanoribbons electron-beam lithography is commonly used for its high resolution. Graphene is exfoliated and deposited onto a substrate, after being located via AFM or SEM, the substrate is then coated with an electron-beam resist, such as poly(methyl methacrylate) (PMMA). Using an enhanced form of SEM and computer software patterns in the PMMA are exposed to impinging electrons to weaken the polymer, enabling it to be removed in the developing stage. This exposes areas of graphene that are removed through reactive ion or oxygen plasma etching. This process is repeated to pattern the sites of electrode deposition by electron-beam evaporation of metal. All

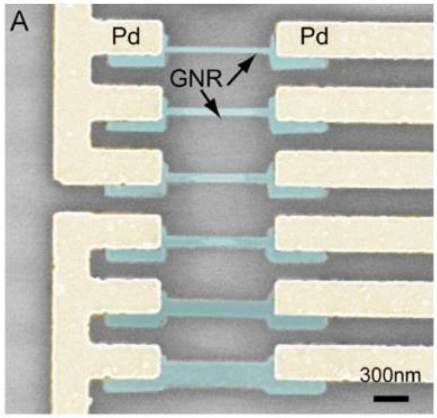

Figure 12: False color SEM image of GNR devices fabricated on a 200nm SiO_2 substrate. The widths of the GNRs from top to bottom are 20, 30, 40, 50, 100 and 200nm. Adapted reference 56 with permission from Elsevier, copyright

remaining photoresist is then removed in a lift off step leaving behind the electrodes and the graphene nanoribbons (Figure 12).[56]

5.1.2 Unzipping of Carbon Nanotubes

Kosynkin et al. were able to unzip commercial multi-walled nanotubes by using permanganate in sulfuric acid.[57] As depicted in Figure 13(left panel), the permanganate and acid oxidize an alkene forming a manganite ester, this is subsequently oxidized further into a dione via dehydration. These buttressing ketones distort the β, γ-alkenes making them more susceptible to permanganate. This repeating process creates a tear or pocket in the nanotube wall. The increasing size of the opening reduces the buttressed ketone strain however, it increases the bond angle strain of the β,γ-alkenes allowing more permanganate attack. This occurs along the alkene axis linearly, as depicted in Figure 13 or along a chiral angle, leaving straight edged graphene nanoribbons.

5.1.3 Plasma Etching

Jiao et at. also used multiwalled nanotubes to create graphene nanoribbons via plasma etching.[58] They began with a multiwalled nanotube solution prepared with 1% Tween 20 sonicated in water, then centrifuged to remove aggregates. The supernatant was deposited onto a silicon substrate, rinsed, dried, then calcined for 10 min at 350°C to remove the Tween 20. The substrate was then spin coated with PMMA and baked for 2 hours at 170°C. The PMMA film was lifted from the substrate in a 1 M potassium hydroxide (KOH) solution and contact printed onto a silicon substrate and adhered by heating for 10 min at 80°C. The film was then subjected to an argon plasma etch (40 mTorr base pressure). By varying the etching time, the multiwalled

nanotubes were broken down to different products: bilayer graphene nanoribbons and carbon nanotubes, tri-, bi-, and single-layer graphene nanoribbons (Figure 13, top right). The remaining PMMA is them removed with acetone vapor leaving behind the nanoribbon products.

5.1.4 Oxidation/Sonication of Nanotubes

A year later Jiao published another procedure for the production of graphene nanoribbons from multiwalled nanotubes.[59] Multiwalled nanotubes were calcined in a tube furnace for 2 hours at 500°C followed by sonication in 1,2-dichloroethane. In the furnace oxygen reacts with pre-existing defect sites etching pits in the multiwalled nanotube sidewalls, then during the solution phase sonication hot gas bubbles enlarge the pits, unzipping the carbon layers into graphene nanoribbons (Figure 13, bottom right).

5.1.5 Bottom-Up Synthesis

A more uniform, bottom-up example of nanoribbon synthesis is shown by Cai et al.[60] This work displays surface assisted coupling of linear polyphenyls, with high topology and width control, by linking monomers of 10,10'-dibromo-9,9'-bianthryl, nanoribbons 7 carbons thick. Firstly, thermal sublimation deposits monomer units on the substrate in the dihalogenated state, surface stabilized biradical intermediates. Heating the substrate to 200°C these molecular units diffuse across the surface and form carbon-carbon bonds. A second thermal treatment at 400°C causes cyclodehydrogenation which creates continuous, aromatic nanoribbons. Graphene nanoribbons are of great interest due to their electronic properties which resemble carbon nanotubes. Due to the width, quantum and edge effects they are semiconducting, making them ideal for nano-transistors.

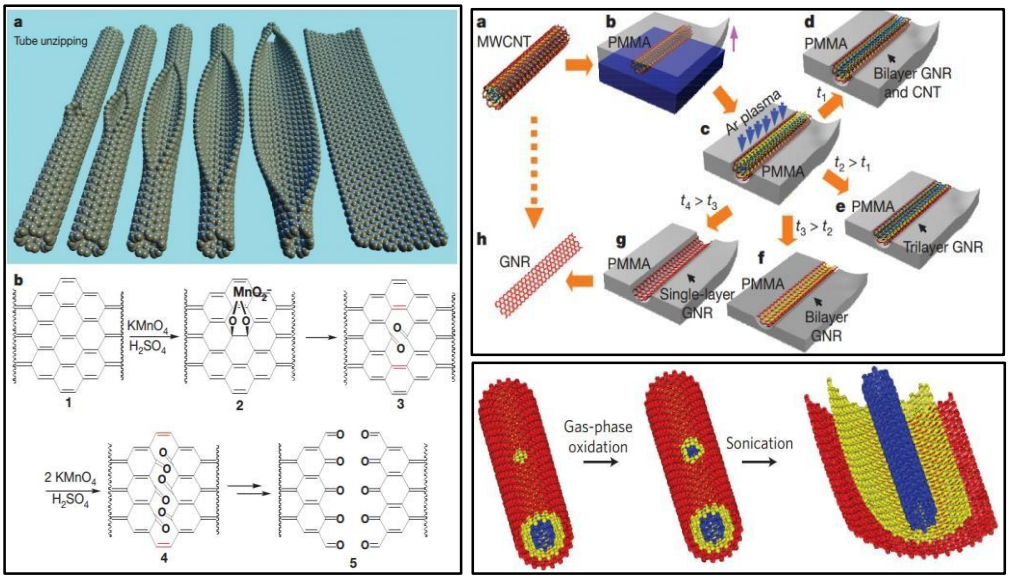

Figure 13: Various methods of graphene nanoribbons production. (Left tile) Gradual chemical unzipping. **(a)** Cartoon representation of gradual unzipping of single-walled nanotube to form nanoribbon, **(b)** chemical mechanism of unzipping process. Adapted from reference 57 with permission from Nature Publishing Group, copyright 2009. (Top right tile) Plasma etching of multiwalled nanotube. **(a)** pristine multiwalled nanotube, **(b)** nanotube on substrate is coated with PMMA, **(c)** PMMA is peeled off substrate and exposed to argon plasma resulting in **(d)** nanoribbons with nanotube cores after short etching time, t_1; tri-, bi- and single layer nanoribbons (e-g, respectively) for etching times $t_{2\text{-}4}$ ($t_1 < t_2 < t_3 < t_4$). **(h)** PMMA is removed to give nanoribbons. Adapted from reference 58 with permission from Nature Publishing Group, copyright 2009. (Bottom right tile) Representation of gas oxidation/liquid unzipping process. Adapted from reference 59, with permission from Nature Publishing Group, copyright 2010.

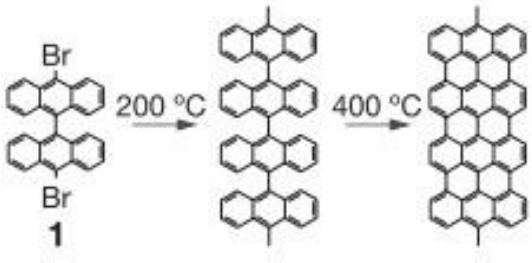

Figure 14: Mechanism of atomically precise graphene nanoribbon synthesis from bianthryl monomer units (1). Adapted from reference 60 with permission from Nature Publishing Group, copyright 2010.

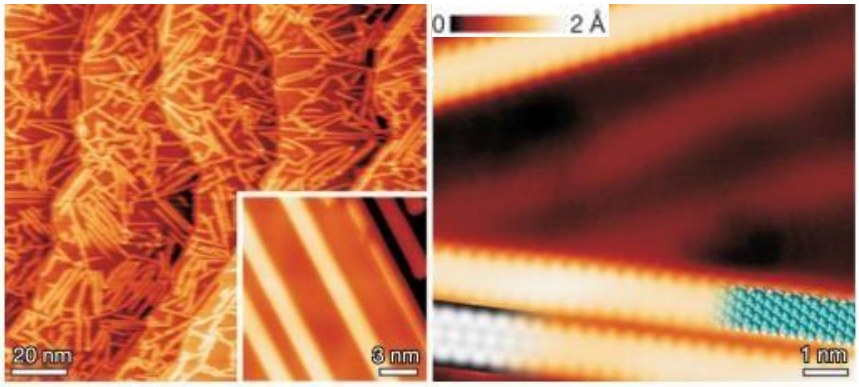

Figure 15: Scanning tunneling micrographs of bottom-up synthesized graphene nanoribbons. Blue and white cartoon spheres represent atoms present in nanoribbon. Adapted from reference 60 with permission from Nature Publishing Group, copyright 2010.

5.2 Electronic Properties of Graphene Nanoribbons

Graphene nanoribbons exhibit unique electronic properties which vary with their width.[56] This arises from the graphitic properties of wide nanoribbons, which have ballistic conductivity of charges, however, when the path is narrowed, edge effects such as electron scattering sites make them more semiconducting. Figure 16a shows typical FET graphs of a 16 nm graphene nanoribbon which exhibits ambipolar properties compared to a 7 nm nanoribbon which exhibits more semi conducting properties (Figure 16b,c).

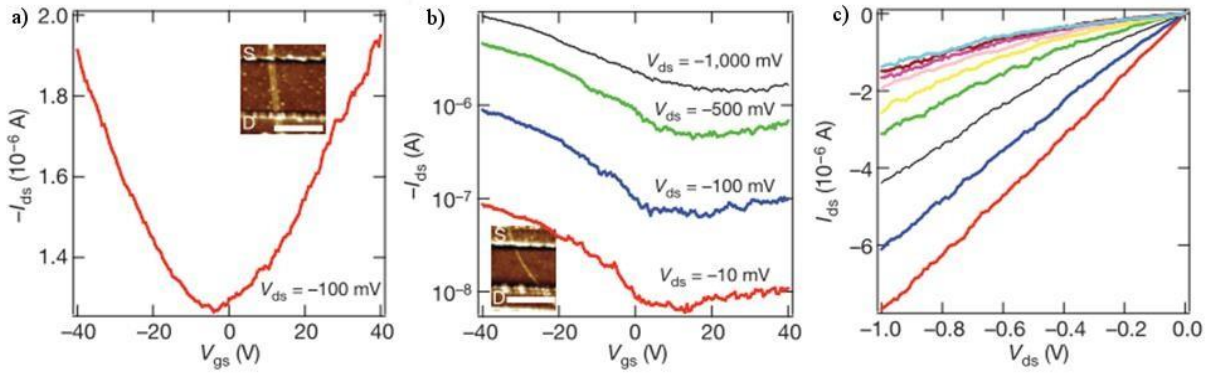

Figure 16: (a) Plot of drain–source current (Ids) versus gate–source voltage (Vgs) for a, 16 nm wide GNR device probed in vacuum after electrical annealing. The Dirac point is near Vg 50 V. Inset, AFM image of this device; scale bar, 200 nm. **(b)** I_{ds}–V_{gs} curves for a 7 nm wide GNR device at various biases probed in air (inset, AFM image; scale bar, 200 nm). The ratio of on-state current (I_{on}) to off-state current (I_{off}) for this GNR device is, 10. **(c)** I_{ds}–V_{ds} curves for the device in (c) at gate biases V_{gs} ranging from 240 V (bottom) to 40 V (top) in steps of 10 V. Adapted from reference 58 with permission from Nature Publishing Group, copyright 2009.

Barone et al. examined the electronic structures of graphene nanoribbons using density functional theory calculations and found that the band gap is dependent not only on the width of the nanoribbon but also the crystallographic direction of their main axis.[61] They found that like armchair carbon nanotubes, nanoribbons that have zig-zag edges are all metallic, whereas armchair nanoribbons are semiconducting. They continue to explain that the width of armchair nanoribbons must be between 2 and 3 nm to make a band gap comparable to germanium (0.67 eV) or indium nitride (0.7 eV), and less than 2 nm to achieve band gaps relative to silicon (1.14 eV) or gallium arsenide (1.43 eV). In the study Barone examined several different nanoribbons derived from the unfolding of carbon nanotubes of different chiralities. The ribbons were

assigned two values for the calculations: L = width, and ϕ = chiral angle. The chiral angle of the nanoribbon corresponds to the nanotube indices (n,m) through the equation

$$\tan(\phi) = (3^{\frac{1}{2}} * \frac{m}{2n+m})$$

Figure 17 shows the nanoribbon configurations that were used to calculate the band gap energies, where each ribbon is depicted as if a carbon nanotube has been unfolded and cut to a particular width and arranged a-e with decreasing chiral angles, ϕ. The calculated band gap energies are shown in the graphs of Figure 18. The left graph shows two types of dynamic functional theory calculations applied to armchair nanoribbons with increasing widths, L. Using the *Gaussian* suite programs and optimized Gaussian basis sets, they then implemented two functionals, the PBE

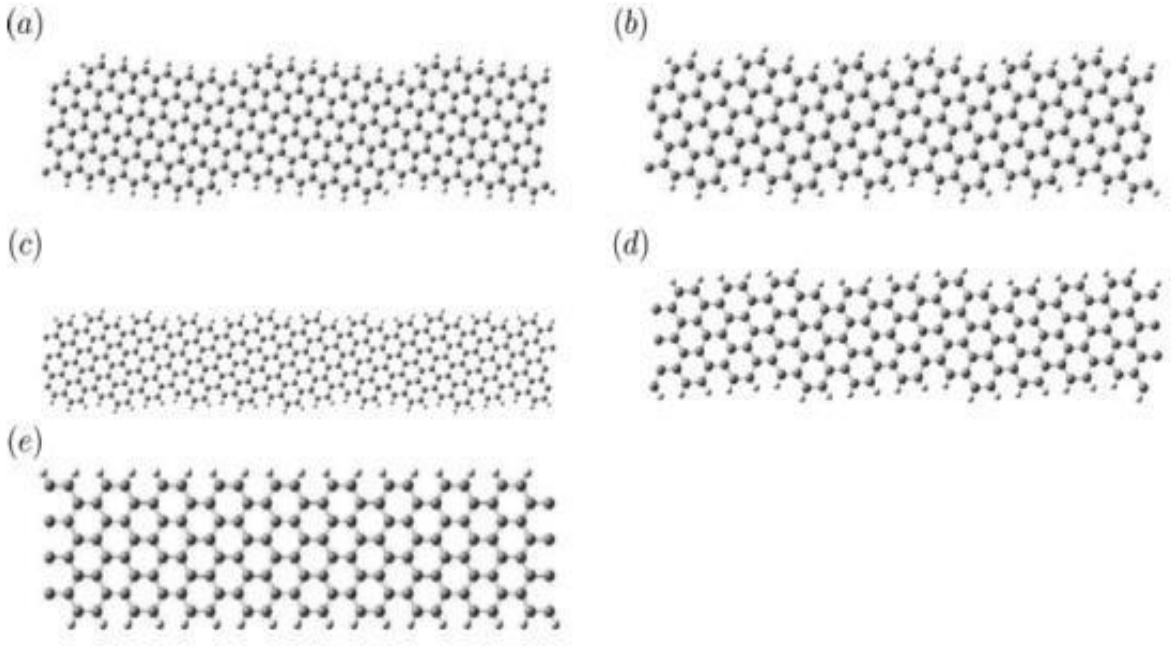

Figure 17: Representations of semiconducting, hydrogen terminated graphene nanoribbons of various chiral angles formed from unfolding and cutting carbon nanotubes. (a) ϕ = 23.4°, from a (6, 4) nanotube. (b) ϕ = 13.9°, from a (6, 2) nanotube. (c) ϕ = 8.9°, from a (20, 4) nanotube. (d) ϕ = 4.7°, from a (10, 1) nanotube. (e) ϕ = 0°, from a zigzag nanotube. Adapted from reference 60 with permission from the American Chemical Society, copyright 2010.

realization of generalized gradient approximation, and the screened exchange hybrid density functional, HSE which has been used to accurately calculate experimental band gaps. These two functionals yielded different values for the increasing width, but they exhibit a similar oscillating pattern. This is attributed to the addition of carbon atoms to the sides of the zigzag axis of the nanoribbon and the corresponding Fermi wavelength of the P_z electrons contributing to the π system.[62] Additions of 3 atoms is on the order of another added wavelength resulting in the 3 fold pattern. The right hand graph of Figure 18 shows the different band gap energy versus ribbon width graphs of the nanoribbons shown in Figure 17. It can be seen that when $\phi = 0°$, there is a larger average band gap. These calculations can help tune the design of device architecture to increase performance.

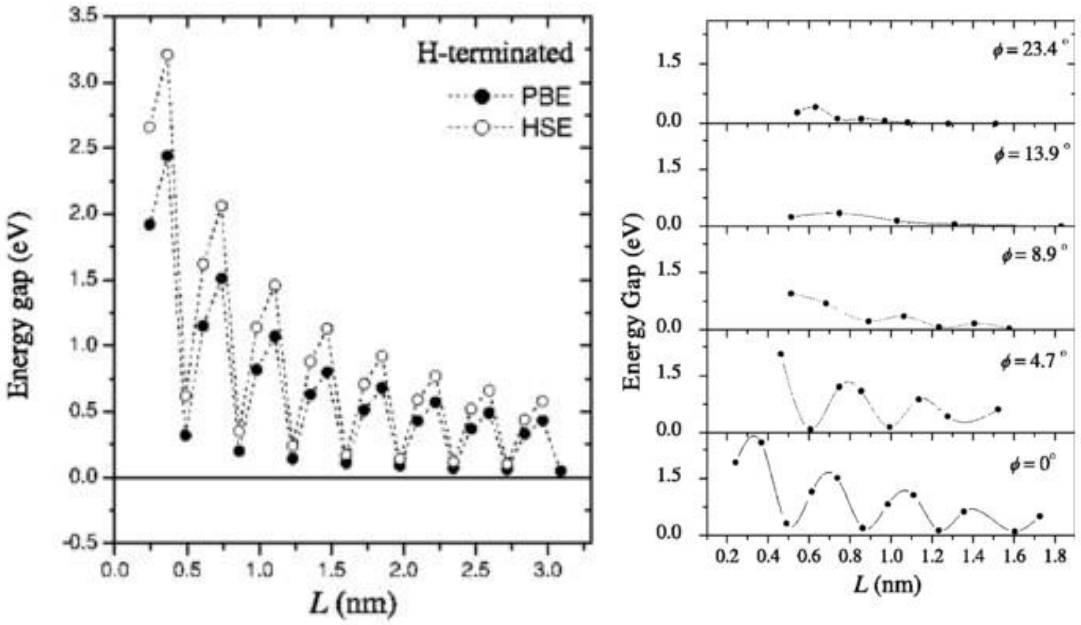

Figure 18: (left) Dependence of the band gap for hydrogen-terminated armchair nanoribbons. (right) Dependence of the band gap on the width of hydrogen passivated chiral graphene nanoribbons. The different panels correspond to the different graphene nanoribbons presented Figure 17. Adapted from reference 60 with permission from the American Chemical copyright 2010.

5.3 Sensor Applications of Graphene Nanoribbons

Like carbon nanotubes, nanoribbons are utilized in sensor arrays to detect gases like hydrogen.[63] Hydrogen is an odorless and hazardous gas due to its low flammability point of 4 % in air. This is of pressing interest due to its use in fuel cells. Sensors are required to detect leaks where fuel cells are used such as spacecraft or some automobiles. It has been shown that palladium greatly increases sensitivity to hydrogen. Molecular hydrogen dissociates to atomic hydrogen at the palladium surface which then dissolves into the metal, lowering the work function of the electron transfer from palladium to carbon nanotubes.[64] Johnson et al. used palladium functionalized multilayer graphene nanoribbon networks as a chemiresistor. Electron beam evaporation was used to deposit a 1 nm layer of palladium over the nanoribbon network, at this thickness the

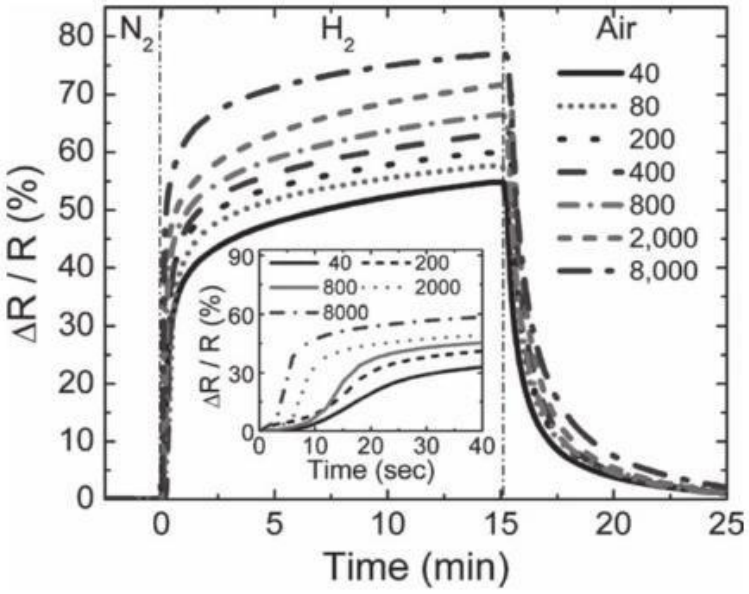

Figure 19: The relative resistance response (ΔR/R) of Pd-functionalized multilayer graphene nanoribbon network sensor as a function of time when exposed to H_2 in N_2 ranging from 40 to 8000 ppm. The inset shows the first 40 seconds of the sensor response for various H_2 concentrations. Adapted from reference 63 with permission from Wiley, copyright 2010.

palladium does not form a continuous thin film forcing conduction through the carbonaceous network.[63] This sensor shows great response at ambient temperatures, approximately 75% increase in relative resistance at high concentrations (8000 ppm H_2) (Figure 19). The Pd-functionalized multilayer graphene nanoribbons show even greater responses at elevated temperatures, this however, requires more energy consumption by the device.

Another functionalized graphene nanoribbon sensor device was used for cancer biomarker sensing.[65] The detection of biomarkers is critical for diagnosis, monitoring, and prevention of diseases. In this work the authors fabricated suspended graphene nanoribbons through a lithographic process to pattern the nanoribbon and HF etching of the underlying silicon wafer. The suspended nanoribbons had a greater sensitivity than unsuspended nanoribbons and graphene sheets to changes in pH (5-9). This heightened sensitivity was also observed when testing for cancer biomarkers. The suspended graphene nanoribbons were functionalized to detect prostate specific antigen (PSA) by incubating a suspended nanoribbon sensor in a solution of poly-l-lysine at room temperature for 1 hour followed by incubation in a solution of anti-PSA antibody in phosphate buffered saline (PBS) overnight, at 4 °C. After the antibody incubation and subsequent PBS rinse the device was passivated with bovine serum albumin, to prevent non- specific binding, for 5 hours then rinsed again in PBS. Sensor devices were tested as FET's and chemiresistors in different concentrations of PSA. In cancer treatment early detection is vital. Therefore, sensors must be very sensitive. These devices made with suspended graphene nanoribbons were capable of detecting 400 fg/mL PSA with greater sensitivity than similarly prepared unsuspended graphene nanoribbons and graphene sheets in both ISFETs and chemiresistors (Figure 20). Figure 20(a) shows the FET response curves to concentrations of PSA. The curves are ambipolar in nature due to the width of the nanoribbon being roughly 50 nm. The suspended graphene nanoribbon is capable of detecting 0.4 pg/mL where unsuspended is only sensitive to 40 pg/mL, which the

authors attribute to the greater surface area available by suspending the nanoribbon, and lack of electronic noise effects from the surface of the SiO_2. Figure 20(c) and (d) show the raw current vs time response data as the concentration of PSA increases, and the average current versus concentration data, respectively.

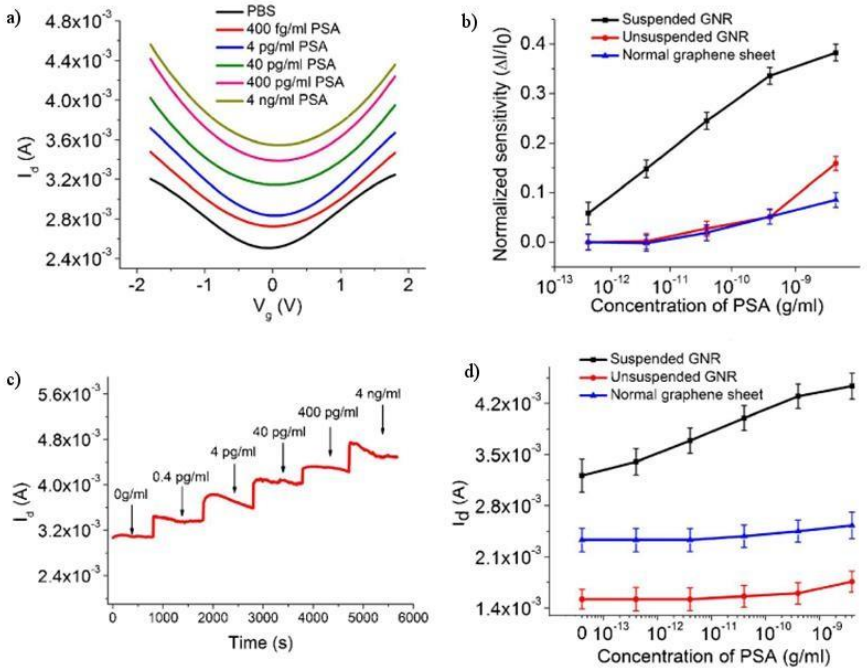

Figure 20: (a) Ambipolar characteristics of suspended GNR ISFET with different PSA solutions induced. The Dirac point of suspended GNR does not shift as significantly as pH detection. **(b)** Normalized sensitivities of different types of ISFETs were measured. Suspended GNR presents the best sensitivity. PBS solution containing no PSA was selected as the reference solution. **(c)** Real-time current change while the different concentrations of PSA solutions were provided to the suspended GNR sensor **(d)** Drain-to-source current versus different PSA concentrations were recorded for different types of ISFET. The results demonstrate that the detection limit of suspended GNR is down to 0.4 pg/mL, compared with the unsuspended GNR and normal graphene with a detection limit of 40 pg/mL. Adapted from reference 65 with permission from IEEE, copyright 2013.

6.0 Holey Reduced Graphene Oxide

6.1 Synthesis

To improve upon a system of nanoribbons one might consider a graphitic network consisting of a single plain with path widths similar to that of a single-walled nanotube or nanoribbon but eliminating the potential barriers at tube-tube/ribbon-ribbon junctions. This is where making porous or holey reduced graphene oxide is beneficial. Graphene is a semimetal due to its band gap.[39, 66] The production of holes creates narrow paths for charge carriers to travel through making the network more semiconducting. Holes can be produced in graphene or graphene oxide sheets a variety of ways. Herein we will examine several methods that include chemical and enzymatic oxidation, and templated etching with block co-polymers or nanoparticles.

6.1.1 Nitric Acid Oxidation

Zhao et al. devised a method through which graphene oxide is suspended in water, mixed with a 70% nitric acid solution and sonicated at room temperature for one hour.[67] After resting for another hour the solution is centrifuged and washed with water to remove acids before vacuum filtration. Varying the ratio of graphene oxide to nitric acid solution yielded varying pore sizes. The holey graphene oxide was then thermally reduced in a tube furnace at 700°C for an hour. Two years later Wang et al. performed a nitric acid reflux reaction on reduced graphene oxide sheets.[68] The reflux used homemade reduced graphene oxide at 0.1 mg/mL and a final nitric acid concentration of 8 M, at 100°C for multiple lengths of time. The size of the pores increased with the reaction time.

6.1.2 Enzymatic Oxidation

It has been shown that peroxidase enzymes can catalyze degradation of carbon nanotubes.[69-71] Kotchey et al. used the enzyme horseradish peroxidase (HRP) to degrade graphene oxide sheets.[72] Here, HRP was incubated with graphene oxide at room temperature in a pH 7 buffer while adding aliquots of hydrogen peroxide daily. The HRP breaks down graphene oxide almost entirely over the course of 20 days. However, after 10 days the incomplete degradation yields sheets with an average pore diameter of 26 nm and neck widths of approximately 9 nm. This method produces sheets of pourous graphene oxide, however, it is in a random manner HRP binding sites are dictated by brownian motion and pore sizes have a wide range of diameters. Procedures to produce repeating patterns, with monodisperse pores and neck widths are desireable to characterize the holey graphene and its properties.

6.1.3 Templated Etching

Several templated methods of nanomesh fabrication have been reported recently. Using a series of etches and depositions Paul et al. were able to create graphene nanomesh with relatively uniform pores roughly 200 nm in diameter.[73] Breifly, graphene was CVD grown from methane or ethanol onto silicon/silica substrates and spincoated with PMMA. The PMMA was then covered with a monolayer of 100 nm diameter polystyrene spheres. The stacked media was then exposed to a short period reactive ion etch to create space between the spheres and subsequently layered with platinum via electron beam evaporation. The remaining polystyrene was then lifted off with 1-chloropentane. This allowed for a second reactive ion etch to remove exposed areas of PMMA/graphene from the areas devoid of platinum. The platinum and remaining PMMA was then removed with acetone leaving the nanomesh on the silica

substrate.

Another patterning approach utilizes block co-polymers.[74] This process begins with graphene flakes on a silica substrate that is then coated with an evaporated silicon oxide later to protect the substrate from the subsequent block co-polymer nanopatterning step. A thin coat of poly(styrene-

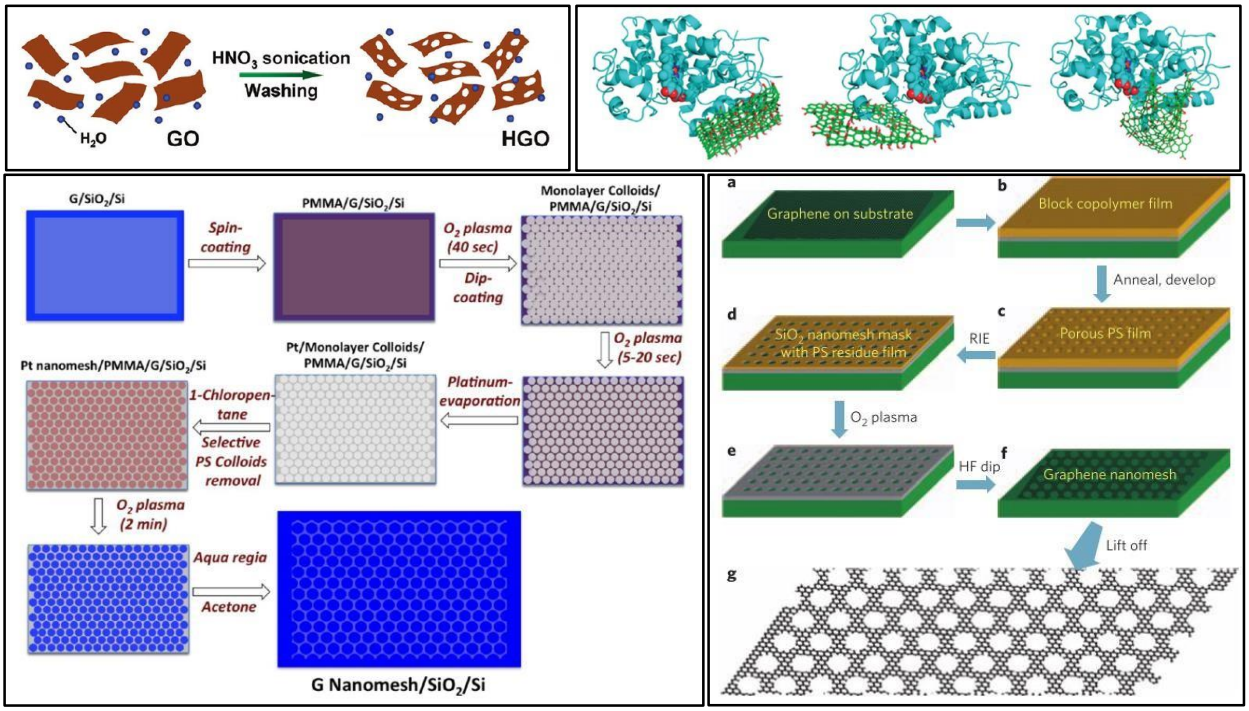

Figure 21: (Top left) representation of introduction of pores into graphene oxide by sonication in nitric acid (not so scale). Adapted from reference 67 with permission from the American Chemical Society copyright 2011. (Top right) computational models of binding poses of HRP on (from left to right) graphene oxide, holey graphene oxide, and a small sheet of graphene oxide calculated using molecular docking studies (AutoDock Vina). Adapted from reference 72 with permission from the American Chemical Society, copyright 2011. (Bottom left) fabrication schematic of graphene nanomesh using polystyrene particle templating. Adapted from reference 73 with permission from the American Chemical Society, copyright 2012. (Bottom right) fabrication schematic using block co-polymers and reactive ion etching. Adapted from reference 74 with permission from Nature Publishing Group, copyright 2010.

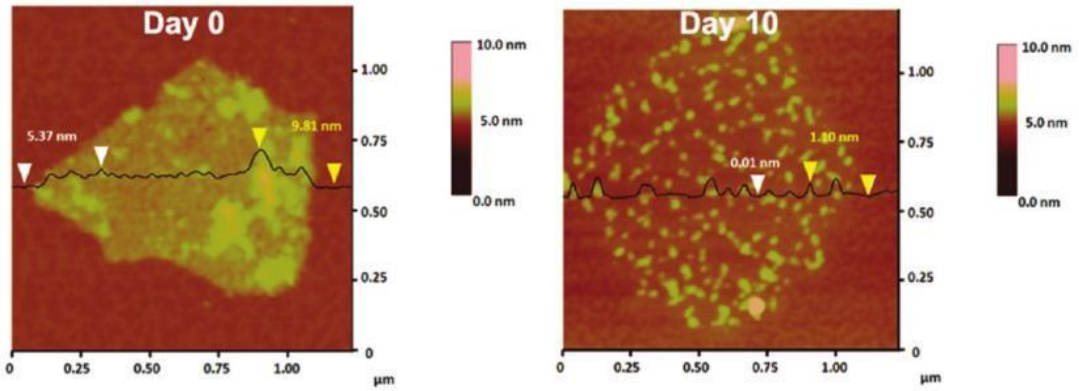

Figure 22: Atomic force micrographs of horse radish peroxidase degraded reduced graphene oxide. Adapted from reference 72 with permission from the American Chemical Society, copyright 2011.

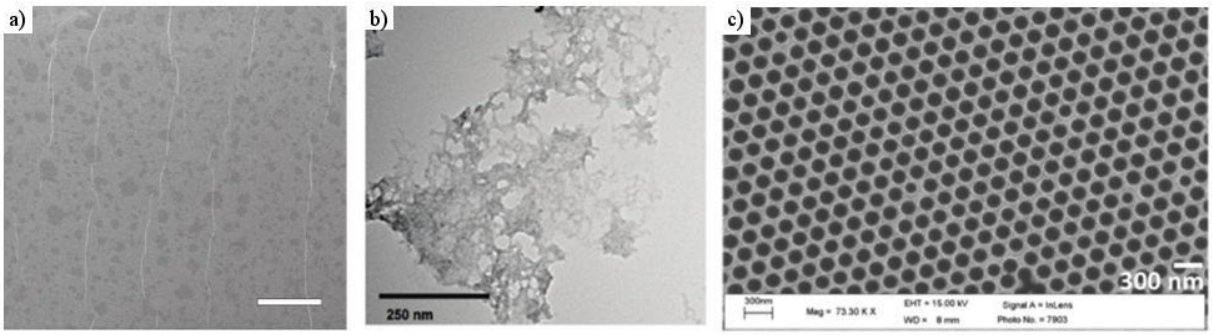

Figure 23: (a) TEM images of holey reduced graphene prepared with nitric acid (adapted from references 66 with permission from the American Chemical Society copyright 2011) and horseradish peroxidase. Adapted from reference 72 with permission from the American Chemical Society, copyright 2011. **(c)** SEM micrograph of graphene nanomesh synthesized particle templating. Adapted from reference 73 with permission from the American Chemical Society, copyright 2012.

block-methyl methacrylate) block copolymer is exposed to ultra violet light to pattern cylindrical domains which are removed in a developing step. The templated structure is then exposed to a fluoroform to bore through the silicon oxide layer, then oxygen reactive ion etch to remove the exposed graphene, creating the nanomesh. The nanomesh was then lifted off the

substrate with hydrofluoric acid and the remaining polymer was removed with acetone vapor.

6.2 Electronic Properties of Holey Reduced Graphene Oxide

Graphene oxide regains is ambipolar FET properties once reduced. Much like the nanoribbons, if the width of the charge carrier path can be narrowed it becomes semiconducting in nature (Figure 27). The presence of holes in the basal plane of the hRGO effectively creates an interconnected network of nanoribbons approximately 9.2± 5.1 nm wide.[75] Other preparations of holey graphene show similar results (Figure 27). Functionalization with platinum nanoparticles yielded an increase in conductance and a positive shift in the Dirac point of the holey reduced graphene oxide.

6.3 Sensor Applications of Holey Reduced Graphene Oxide

Holey graphene is ideal for use in sensors due to its interconnected network of sp^2 carbon. Studies of holey graphene have shown great promise in the field of environmental sensors. A common application for graphene and its derivatives is gas sensing due to its nanoscale size, allowing miniaturized devices that require less operating power, and its ability to be functionalized for specific targets. Graphene nanomeshes synthesized by polystyrene nanoparticle templated etching was also tested for use in gas sensing. Paul et. al. tested the nanomeshes they produced using methane and ethanol CVD grown graphene sheets.[73] Figure 28 shows the resistance versus time graphs and calibration curves of these experiments when testing nanomeshes against increasing concentrations of NO_2 and NH_3 (Figure 28 (a) and (c), respectively). Nanomeshes produced with ethanol showed the greatest response to the gasses, which are opposite in resistance response due to the electron accepting or donating properties of

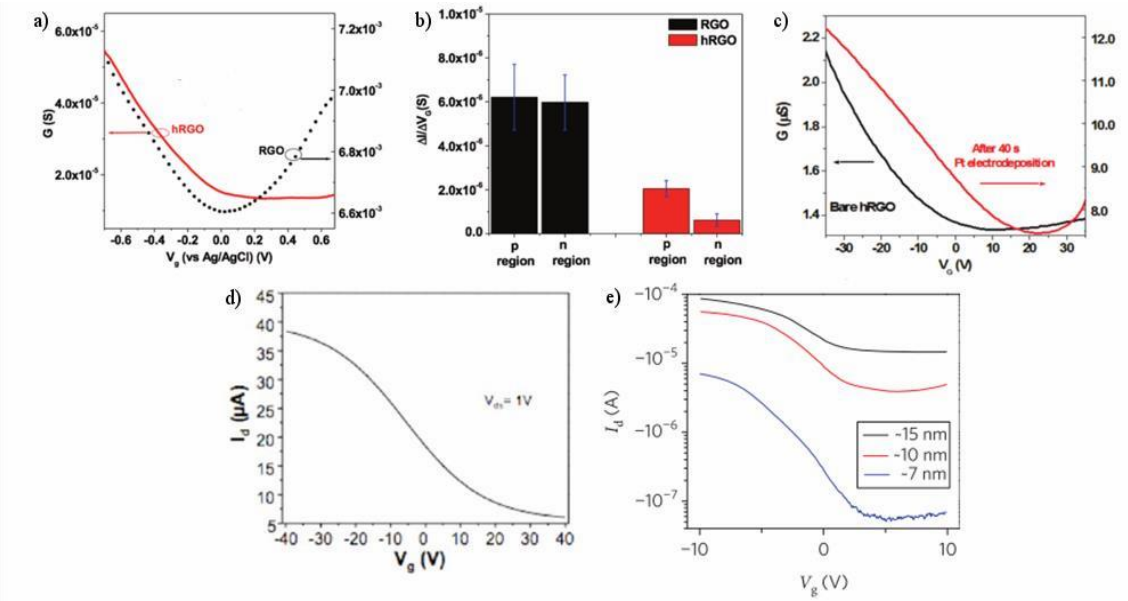

Figure 24: (a) Conductivity versus potential (liquid gate) plot for reduced graphene oxide (RGO, black circles) and holey reduced graphene oxide (hRGO, solid red line). The measurements were recorded in 10 mM KCl/10 mM PBS (pH 7) at a constant V_{ds} of 10 mV. **(b)** Comparison of transconductance ($\Delta I/\Delta V_g$) values of n and p region of 12 different RGO and hRGO FET devices (6 devices each). Adapted from reference 72 with permission from the American Chemical Society, copyright 2011. **(c)** Room-temperature (FET) characteristics (source-drain conductance, G, versus back gate voltage, V_G) of hRGO before and after 40s Pt electrodeposition. A constant V_{ds}) of 50mV was applied. Adapted from reference 75 with permission from the American Chemical Society, copyright 2011. **(d)** source-drain current (I_d) as a function of gate potential (V_g) at constant V_{ds} of 1 V. Adapted from reference 73 with permission from the American Chemical Society, copyright 2012. **(e)** Transfer characteristics at V_d 2100mV for GNMs with different estimated neck widths of ~15 nm (device channel width 6.5 mm and length 3.6 mm), ~10 nm (channel width 2 mm and length 1 mm) and ~7 nm (channel w x l= 3 x 2.3 mm). Adapted from reference 74 with permission from Nature Publishing Group, copyright 2010.

the analyte gas. For the oxidizing gas NO_2, the chemiresistor exhibits a decrease in resistance due

to the increase of holes transporting through the nanomesh. The opposite is seen for the reducing gas NH_3 in which an increase in resistance is observed. This is because the nanomesh acts like a p-type semiconductor and can therefore identify the difference in the oxidative properties of impinging gasses. Further functionalization of the material is needed for producing a specific

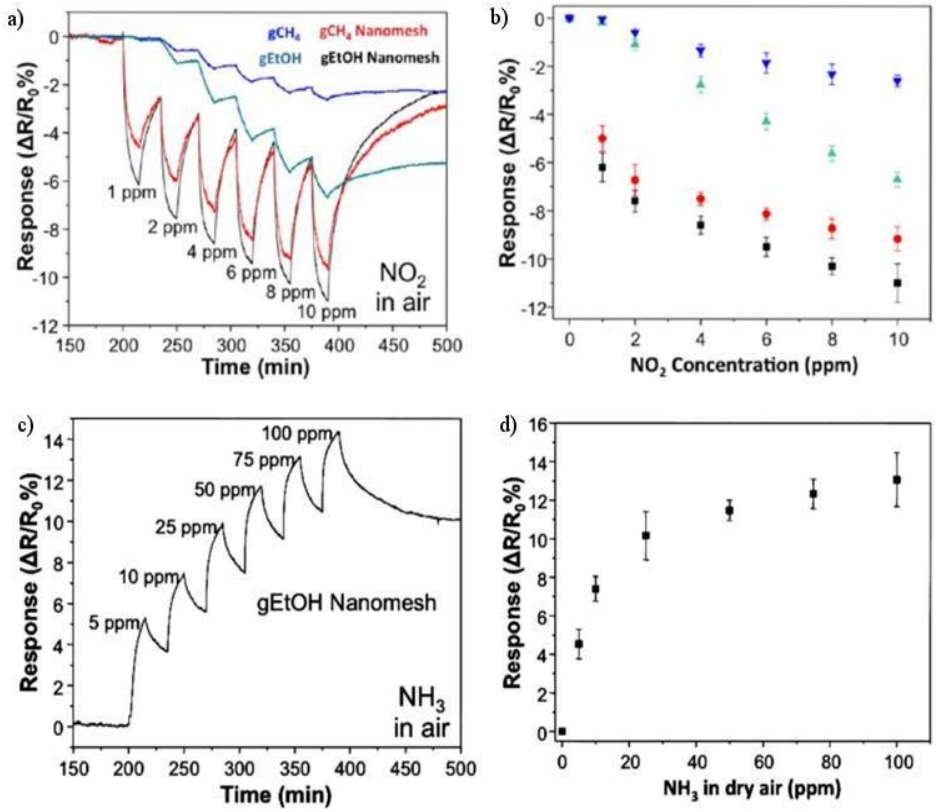

Figure 25: (a) Comparison of dynamic responses of sensor devices fabricated from gCH_4 and gEtOH nanomesh and their continuous film counterparts exposed to various concentrations NO_2 in dry air ranging from 1 to 10 ppm. **(b)** Calibration curves of gCH_4 and gEtOH sensor devices in various concentrations of NO_2 in dry air. **(c,d)** Room temperature NH_3 detection of GNM sensor, dynamic response and calibration curve (respectively) of a gEtOH nanomesh sensor device exposed to various concentrations of NH_3 in dry air ranging from 5 to 100 ppm. Adapted from reference 73 with permission from the American Chemical Society, copyright 2012.

sensor.

Holey graphene synthesized by the aforementioned enzymatic oxidation was used as the transducing element in several experiments to test its response to several gasses and even biological samples. Holey graphene, prepared by enzymatic degradation, has been functionalized with platinum particles for the detection of hydrogen gas.[75] Briefly, hRGO flakes were deposited on interdigitated electrodes using a dielectrophoresis technique until the sensor had an initial conductance of 1-100 µS. The edges and defect sites were decorated with platinum nanoparticles by pulsed potentiostatic electrodeposition. This was performed in a miniature fluid chamber secured to the microchip. With the hRGO acting as the working electrode, a Ag/AgCl (3 M KCl) reference electrode, and a platinum auxiliary electrode, the working electrode was immersed into a 1 mM H_2PtCl_6 solution at a potential of 0.8 V versus Ag/AgCl. The potential was then moved toward the deposition potential of -0.7 V for a time between 10 and 60 seconds, plating nanoparticles of varying sizes onto the hRGO. Figure 29(a) shows an SEM image of a Pt nanoparticle functionalized hRGO sheet upon a gold electrode. Control experiments were performed in similar methods with deposition of gold nanoparticles on hRGO. Pt nanoparticle

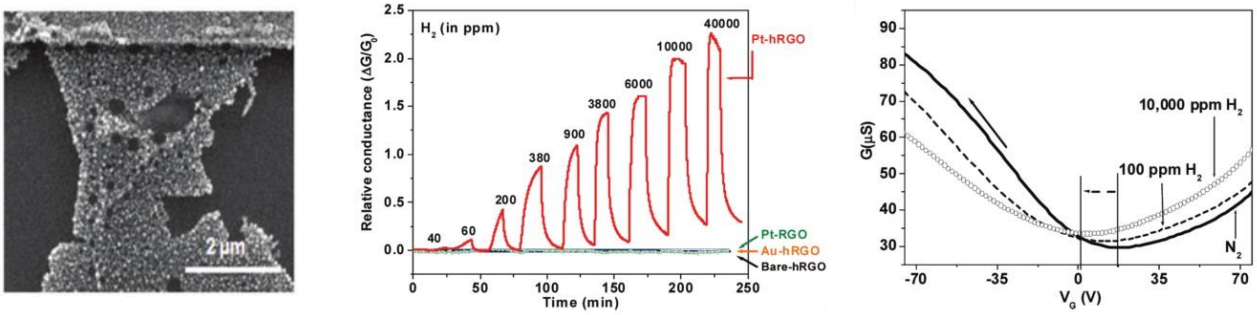

Figure 26: (a) SEM of Pt NP decorated hRGO, **(b)** relative conductance changes of hRGO, NP decorated hRGO, Pt NP decorated RGO, and Pt NP decorated hRGO. **(c)** FET curves of hRGO in 0, 100, and 10000 ppm H_2. Adapted from reference 75 with permission from American Chemical Society, copyright

decorated hRGO showed an enhanced esponse to H_2 gas concentrations, with a limit of detection of 60 ppm. This is close to palladium decorated graphene nanoribbons networks which exhibited a limit of detection of 40 ppm. Platinum decorated RGO, however, did not show any significant response to H_2 gas at room temperature within the experimental range (40-40000 ppm H_2), proving that the porous carbon network and platinum makes a more effective sensor.

The same hRGO, produced by enzymatic oxidation (8 days), was used by Chen et. al. to produce a gram-negative specific bacteria sensor.[30] hRGO was deposited via dielectrophoresis (10 V, 300 kHz, 60 s) and subsequently incubated in EDC and NHS (1 hr) to activate the remaining carboxylic sites. The activated devices were then immersed in a buffered solution containing an antimicrobial peptide (AMP) with a gram-negative specific sequence overnight. Figure 25(a) shows a schematic of the AMP functionalized hRGO FET device bound to bacteria, (b) is an SEM image of 2 bacteria cells immobilized on the device itself, and (c) shows the response characteristics of the device to varying concentrations of *E. coli*. AMP functionalization was confirmed by a decrease in conductance of the p-type region of the FET curve. To prevent nonspecific binding of bacteria to unfunctionalized, exposed hRGO the devices were incubated in a blocking buffer of 0.1 wt% Tween 20 for 1 hr. After thorough rinsing the devices were tested against 10^4 through 10^7 colony forming units (cfu)/mL of *E. coli* and *Lysteria*, gram- negative and gram-positive respectively, with significant responses to gram-negative bacteria and no discernable response to the gram-positive samples. These particular devices were calculated to have a limit of detection of 803 cfu/mL. This type of device may prove helpful in the future for testing for disease causing bacteria.

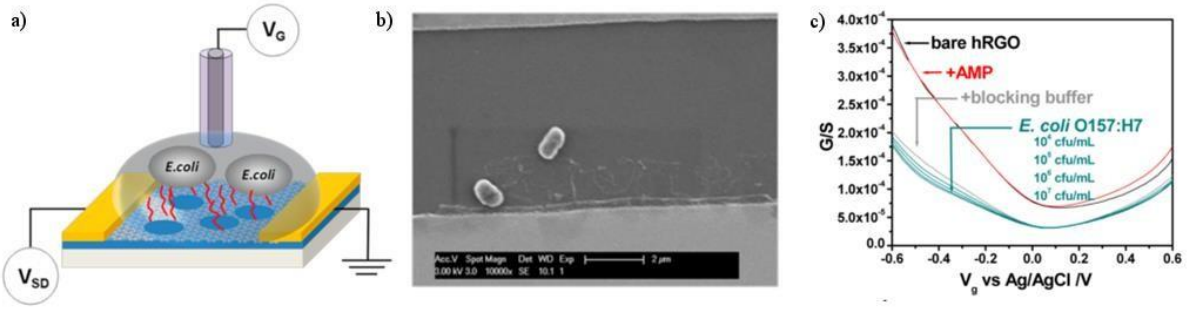

Figure 27: Detection of bacteria using holey reduced graphene oxide. **(a)** Schematic of bacteria specific FET device, **(b)** SEM image of immobilized bacteria on AMP functionalized hRGO, **(c)** FET response to varying concentrations of *E. coli*. Adapted from reference 30 with permission from the American Chemical Society, copyright 2014.

7.0 Outlook and Prospects

In summary, carbon nanomaterials exhibit unique properties that make them ideal for their use as transducing elements in sensor platforms. The carbon nanotube, with is high aspect ratio, allows a band gap (depending on the chiral aspect of the atomic arrangement). This structure can be mimicked by graphene and reduced graphene oxide by narrowing the conduction path of the charge carriers. When the width decreases the semiconducting nature increases, comparable to semiconducting metals or metal oxides at widths small enough. We have also seen that these materials can be functionalized to make sensors specific for particular analytes such as molecules, biomarkers, toxic or hazardous gasses, and even bacteria cells. Furthermore, nanomaterials allow for the miniaturization of sensors, making them more portable for use in the field or point of care applications.

Bibliography

1. Kauffman, D. R. and Star, A. Carbon Nanotube Gas and Vapor Sensors. *Angewandte Chemie International Edition* **47**, 6550-6570 (2008)
2. Heller, I., Janssens, A. M., Mannik, J., Minot, E. D., Lemay, S. G. and Dekker, C. Identifying the mechanism of biosensing with carbon nanotube transistors. *Nano Letters* **8**, 591-595 (2008)
3. Gou, P., Kraut, N. D., Feigel, I. M., Bai, H., Morgan, G. J., Chen, Y., Tang, Y., Bocan, K., Stachel, J., Berger, L., Mickle, M., Sejdić, E. and Star, A. Carbon Nanotube Chemiresistor for Wireless pH Sensing. *Sci. Rep.* **4**, (2014)
4. Geim, A. K. and Novoselov, K. S. The rise of graphene. *Nat Mater* **6**, 183-191 (2007)
5. H. W. Kroto, J. R. H., S. C. O'Brien, R. F. Curl & R. E. Smalley. C60: Buckminsterfullerene. *Nature* **318**, 162-163 (1985)
6. Paredes, J. I., Martinez-Alonso, A. and Tascon, J. M. D. Application of scanning tunneling and atomic force microscopies to the characterization of microporous and mesoporous materials. *Microporous Mesoporous Mat.* **65**, 93-126 (2003)
7. Giessibl, F. J., Hembacher, S., Bielefeldt, H. and Mannhart, J. Subatomic features on the silicon (111)-(7x7) surface observed by atomic force microscopy. *Science* **289**, 422-425 (2000)
8. Thomsen, C. and Reich, S. Double Resonant Raman Scattering in Graphite. *Physical Review Letters* **85**, 5214-5217 (2000)
9. Nan, H. Y., Ni, Z. H., Wang, J., Zafar, Z., Shi, Z. X. and Wang, Y. Y. The thermal stability of graphene in air investigated by Raman spectroscopy. *Journal of Raman Spectroscopy* **44**, 1018-1021 (2013)
10. Balasubramanian, K. and Burghard, M. Chemically Functionalized Carbon Nanotubes. *Small* **1**, 180-192 (2005)
11. Chartuprayoon, N., Zhang, M., Bosze, W., Choa, Y.-H. and Myung, N. V. One-dimensional nanostructures based bio-detection. *Biosensors & Bioelectronics* **63**, 432-443 (2015)
12. Feigel, I. M., Vedala, H. and Star, A. Biosensors based on one-dimensional nanostructures. *Journal of Materials Chemistry* **21**, 8940-8954 (2011)
13. Das, R., Hamid, S. B. A., Ali, M. E., Ismail, A. F., Annuar, M. S. M. and Ramakrishna, S. Multifunctional carbon nanotubes in water treatment: The present, past and future. *Desalination* **354**, 160-179 (2014)
14. Xiong, L. and Compton, R. G. Amperometric Gas detection: A Review. *Int. J. Electrochem. Sci.* **9**, 7152-7181 (2014)
15. Chen, Y., Vedala, H., Kotchey, G. P., Audfray, A., Cecioni, S., Imberty, A., Vidal, S. and Star, A. Electronic Detection of Lectins Using Carbohydrate-Functionalized Nanostructures: Graphene versus Carbon Nanotubes. *ACS Nano* **6**, 760-770 (2011)
16. Vedala, H., Chen, Y., Cecioni, S., Imberty, A., Vidal, S. b. and Star, A. Nanoelectronic Detection of Lectin-Carbohydrate Interactions Using Carbon Nanotubes. *Nano Letters* **11**, 170-175 (2011)
17. Münzer, A. M., Seo, W., Morgan, G. J., Michael, Z. P., Zhao, Y., Melzer, K., Scarpa, G. and Star, A. Sensing Reversible Protein–Ligand Interactions with Single-Walled Carbon

Nanotube Field-Effect Transistors. *The Journal of Physical Chemistry C* **118**, 17193-17199 (2014)
18. Allen, B. L., Kichambare, P. D. and Star, A. Carbon Nanotube Field-Effect-Transistor-Based Biosensors. *Advanced Materials* **19**, 1439-1451 (2007)
19. Star, A., Tu, E., Niemann, J., Gabriel, J.-C. P., Joiner, C. S. and Valcke, C. Label-free detection of DNA hybridization using carbon nanotube network field-effect transistors. *Proceedings of the National Academy of Sciences of the United States of America* **103**, 921-926 (2006)
20. Star, A., Gabriel, J.-C. P., Bradley, K. and Grüner, G. Electronic Detection of Specific Protein Binding Using Nanotube FET Devices. *Nano Letters* **3**, 459-463 (2003)
21. Ding, M., Sorescu, D. C. and Star, A. Photoinduced Charge Transfer and Acetone Sensitivity of Single-Walled Carbon Nanotube–Titanium Dioxide Hybrids. *J. Am. Chem. Soc.* **135**, 9015-9022 (2013)
22. Ding, M. and Star, A. Selecting Fruits with Carbon Nanotube Sensors. *Angewandte Chemie International Edition* **51**, 7637-7638 (2012)
23. Ding, M., Sorescu, D. C., Kotchey, G. P. and Star, A. Welding of Gold Nanoparticles on Graphitic Templates for Chemical Sensing. *J. Am. Chem. Soc.* **134**, 3472-3479 (2012)
24. Kauffman, D. R., Shade, C. M., Uh, H., Petoud, S. and Star, A. Decorated carbon nanotubes with unique oxygen sensitivity. *Nat Chem* **1**, 500-506 (2009)
25. Kauffman, D. R. and Star, A. Simultaneous Spectroscopic and Solid-State Electronic Measurement of Single-Walled Carbon Nanotube Devices. *The Journal of Physical Chemistry C* **112**, 4430-4434 (2008)
26. Star, A., Han, T. R., Joshi, V., Gabriel, J. C. P. and Grüner, G. Nanoelectronic Carbon Dioxide Sensors. *Advanced Materials* **16**, 2049-2052 (2004)
27. Gou, P., Kraut, N. D., Feigel, I. M. and Star, A. Rigid versus flexible ligands on carbon nanotubes for the enhanced sensitivity of cobalt ions. *Macromolecules* **46**, 1376-1383 (2013)
28. Chen, Y., Lee, Y. D., Vedala, H., Allen, B. L. and Star, A. Exploring the Chemical Sensitivity of a Carbon Nanotube/Green Tea Composite. *ACS Nano* **4**, 6854-6862 (2010)
29. Vlandas, A., Kurkina, T., Ahmad, A., Kern, K. and Balasubramanian, K. Enzyme-Free Sugar Sensing in Microfluidic Channels with an Affinity-Based Single-Wall Carbon Nanotube Sensor. *Analytical Chemistry* **82**, 6090-6097 (2010)
30. Chen, Y., Michael, Z. P., Kotchey, G. P., Zhao, Y. and Star, A. Electronic Detection of Bacteria Using Holey Reduced Graphene Oxide. *ACS Applied Materials & Interfaces* **6**, 3805-3810 (2014)
31. Bethune, D. S., Klang, C. H., de Vries, M. S., Gorman, G., Savoy, R., Vazquez, J. and Beyers, R. Cobalt-catalysed growth of carbon nanotubes with single-atomic-layer walls. *Nature* **363**, 605-607 (1993)
32. Guo, T., Nikolaev, P., Rinzler, A. G., Tomanek, D., Colbert, D. T. and Smalley, R. E. Self-Assembly of Tubular Fullerenes. *The Journal of Physical Chemistry* **99**, 10694-10697 (1995)
33. Cassell, A. M., Raymakers, J. A., Kong, J. and Dai, H. J. Large scale CVD synthesis of single-walled carbon nanotubes. *Journal of Physical Chemistry B* **103**, 6484-6492 (1999)
34. Novoselov, K. S., Geim, A. K., Morozov, S. V., Jiang, D., Zhang, Y., Dubonos, S. V., Grigorieva, I. V. and Firsov, A. A. Electric field effect in atomically thin carbon films. *Science* **306**, 666-669 (2004)
35. Zhao, W., Fang, M., Wu, F., Wu, H., Wang, L. and Chen, G. Preparation of graphene by exfoliation of graphite using wet ball milling. *Journal of Materials Chemistry* **20**, 5817-5819 (2010)

36. Hummers, W. S. and Offeman, R. E. PREPARATION OF GRAPHITIC OXIDE. *J. Am. Chem. Soc.* **80**, 1339-1339 (1958)
37. Marcano, D. C., Kosynkin, D. V., Berlin, J. M., Sinitskii, A., Sun, Z. Z., Slesarev, A., Alemany, L. B., Lu, W. and Tour, J. M. Improved Synthesis of Graphene Oxide. *Acs Nano* **4**, 4806-4814 (2010)
38. Stankovich, S., Dikin, D. A., Piner, R. D., Kohlhaas, K. A., Kleinhammes, A., Jia, Y., Wu, Y., Nguyen, S. T. and Ruoff, R. S. Synthesis of graphene-based nanosheets via chemical reduction of exfoliated graphite oxide. *Carbon* **45**, 1558-1565 (2007)
39. Novoselov, K. S., Geim, A. K., Morozov, S. V., Jiang, D., Katsnelson, M. I., Grigorieva, I. V., Dubonos, S. V. and Firsov, A. A. Two-dimensional gas of massless Dirac fermions in graphene. *Nature* **438**, 197-200 (2005)
40. Kaempgen, M. and Roth, S. Transparent and flexible carbon nanotube/polyaniline pH sensors. *Journal of Electroanalytical Chemistry* **586**, 72-76 (2006)
41. Ferrer-Anglada, N., Kaempgen, M. and Roth, S. Transparent and flexible carbon nanotube/polypyrrole and carbon nanotube/polyaniline pH sensors. *Physica Status Solidi B: Basic Solid State Physics* **243**, 3519-3523 (2006)
42. Kim, K. S., Zhao, Y., Jang, H., Lee, S. Y., Kim, J. M., Kim, K. S., Ahn, J. H., Kim, P., Choi, J. Y. and Hong, B. H. Large-scale pattern growth of graphene films for stretchable transparent electrodes. *Nature* **457**, 706-710 (2009)
43. Tang, Y. F., Kotchey, G. P., Vedala, H. and Star, A. Electrochemical Detection with Platinum Decorated Carbon Nanomaterials. *Electroanalysis* **23**, 870-877 (2011)
44. Wanekaya, A. K., Chen, W., Myung, N. V. and Mulchandani, A. Nanowire-based electrochemical biosensors. *Electroanalysis* **18**, 533-550 (2006)
45. Wallace, P. R. THE BAND THEORY OF GRAPHITE. *Physical Review* **71**, 476-476 (1947)
46. Nemade, K. R. and Waghuley, S. A. Chemiresistive Gas Sensing by Few-Layered Graphene. *Journal of Electronic Materials* **42**, 2857-2866 (2013)
47. Li, P., Lei, N., Xu, J. and Xue, W. High-Yield Fabrication of Graphene Chemiresistors With Dielectrophoresis. *Ieee Transactions on Nanotechnology* **11**, 751-759 (2012)
48. Zhang, G., Guo, X., Wang, S., Wang, X., Zhou, Y. and Xu, H. New graphene fiber coating for volatile organic compounds analysis. *Journal of Chromatography B-Analytical Technologies in the Biomedical and Life Sciences* **969**, 128-131 (2014)
49. Quang, V. V., Hung, V. N., Tuan, L. A., Phan, V. N., Huy, T. Q. and Quy, N. V. Graphene-coated quartz crystal microbalance for detection of volatile organic compounds at room temperature. *Thin Solid Films* **568**, 6-12 (2014)
50. Huang, Q., Zeng, D., Li, H. and Xie, C. Room temperature formaldehyde sensors with enhanced performance, fast response and recovery based on zinc oxide quantum dots/graphene nanocomposites. *Nanoscale* **4**, 5651-5658 (2012)
51. Meng, F.-L., Li, H.-H., Kong, L.-T., Liu, J.-Y., Jin, Z., Li, W., Jia, Y., Liu, J.-H. and Huang, X.-J. Parts per billion-level detection of benzene using SnO2/graphene nanocomposite composed of sub-6 nm SnO2 nanoparticles. *Analytica Chimica Acta* **736**, 100-107 (2012)
52. Nemade, K. R. and Waghuley, S. A. Highly responsive carbon dioxide sensing by graphene/Al2O3 quantum dots composites at low operable temperature. *Indian Journal of Physics* **88**, 577-583 (2014)
53. Timmer, B., Olthuis, W. and van den Berg, A. Ammonia sensors and their applications - a review. *Sensors and Actuators B-Chemical* **107**, 666-677 (2005)

54. Yoo, S., Li, X., Wu, Y., Liu, W., Wang, X. and Yi, W. Ammonia Gas Detection by Tannic Acid Functionalized and Reduced Graphene Oxide at Room Temperature. *Journal of Nanomaterials* (2014)
55. Yang, Y., Yang, X., Yang, W., Li, S., Xu, J. and Jiang, Y. Porous conducting polymer and reduced graphene oxide nanocomposites for room temperature gas detection. *Rsc Advances* **4**, 42546-42553 (2014)
56. Chen, Z. H., Lin, Y. M., Rooks, M. J. and Avouris, P. Graphene nano-ribbon electronics. *Physica E* **40**, 228-232 (2007)
57. Kosynkin, D. V., Higginbotham, A. L., Sinitskii, A., Lomeda, J. R., Dimiev, A., Price, B. K. and Tour, J. M. Longitudinal unzipping of carbon nanotubes to form graphene nanoribbons. *Nature* **458**, 872-U5 (2009)
58. Jiao, L., Zhang, L., Wang, X., Diankov, G. and Dai, H. Narrow graphene nanoribbons from carbon nanotubes. *Nature* **458**, 877-880 (2009)
59. Jiao, L., Wang, X., Diankov, G., Wang, H. and Dai, H. Facile synthesis of high-quality graphene nanoribbons. *Nature Nanotechnology* **5**, 321-325 (2010)
60. Cai, J., Ruffieux, P., Jaafar, R., Bieri, M., Braun, T., Blankenburg, S., Muoth, M., Seitsonen, A. P., Saleh, M., Feng, X., Muellen, K. and Fasel, R. Atomically precise bottom-up fabrication of graphene nanoribbons. *Nature* **466**, 470-473 (2010)
61. Barone, V., Hod, O. and Scuseria, G. E. Electronic structure and stability of semiconducting graphene nanoribbons. *Nano Letters* **6**, 2748-2754 (2006)
62. Nakada, K., Fujita, M., Dresselhaus, G. and Dresselhaus, M. S. Edge state in graphene ribbons: Nanometer size effect and edge shape dependence. *Phys. Rev. B* **54**, 17954-17961 (1996)
63. Johnson, J. L., Behnam, A., Pearton, S. J. and Ural, A. Hydrogen Sensing Using Pd-Functionalized Multi-Layer Graphene Nanoribbon Networks. *Advanced Materials* **22**, 4877-+ (2010)
64. Kong, J., Chapline, M. G. and Dai, H. J. Functionalized carbon nanotubes for molecular hydrogen sensors. *Advanced Materials* **13**, 1384-1386 (2001)
65. Zhang, B. and Cui, T. Suspended Graphene Nanoribbon Ion-Sensitive Field-Effect Transistors Formed by Shrink Lithography for pH/Cancer Biomarker Sensing. *Journal of Microelectromechanical Systems* **22**, 1140-1146 (2013)
66. Meric, I., Han, M. Y., Young, A. F., Ozyilmaz, B., Kim, P. and Shepard, K. L. Current saturation in zero-bandgap, topgated graphene field-effect transistors. *Nature Nanotechnology* **3**, 654-659 (2008)
67. Zhao, X., Hayner, C. M., Kung, M. C. and Kung, H. H. Flexible Holey Graphene Paper Electrodes with Enhanced Rate Capability for Energy Storage Applications. *Acs Nano* **5**, 8739-8749 (2011)
68. Wang, X. L., Jiao, L. Y., Sheng, K. X., Li, C., Dai, L. M. and Shi, G. Q. Solution-processable graphene nanomeshes with controlled pore structures. *Scientific Reports* **3**, 5 (2013)
69. Allen, B. L., Kotchey, G. P., Chen, Y., Yanamala, N. V. K., Klein-Seetharaman, J., Kagan, V. E. and Star, A. Mechanistic Investigations of Horseradish Peroxidase-Catalyzed Degradation of Single-Walled Carbon Nanotubes. *J. Am. Chem. Soc.* **131**, 17194-17205 (2009)
70. Allen, B. L., Kichambare, P. D., Gou, P., Vlasova, I. I., Kapralov, A. A., Konduru, N., Kagan, V. E. and Star, A. Biodegradation of Single-Walled Carbon Nanotubes through Enzymatic Catalysis. *Nano Letters* **8**, 3899-3903 (2008)

71. Kagan, V. E., Konduru, N. V., Feng, W., Allen, B. L., Conroy, J., Volkov, Y., Vlasova, I. I., Belikova, N. A., Yanamala, N., Kapralov, A., Tyurina, Y. Y., Shi, J., Kisin, E. R., Murray, A. R., Franks, J., Stolz, D., Gou, P., Klein-Seetharaman, J., Fadeel, B., Star, A. and Shvedova, A. A. Carbon nanotubes degraded by neutrophil myeloperoxidase induce less pulmonary inflammation. *Nat Nano* **5**, 354-359 (2010)
72. Kotchey, G. P., Allen, B. L., Vedala, H., Yanamala, N., Kapralov, A. A., Tyurina, Y. Y., Klein-Seetharaman, J., Kagan, V. E. and Star, A. The Enzymatic Oxidation of Graphene Oxide. *ACS Nano* **5**, 2098-2108 (2011)
73. Paul, R. K., Badhulika, S., Saucedo, N. M. and Mulchandani, A. Graphene Nanomesh As Highly Sensitive Chemiresistor Gas Sensor. *Analytical Chemistry* **84**, 8171-8178 (2012)
74. Bai, J., Zhong, X., Jiang, S., Huang, Y. and Duan, X. Graphene nanomesh. *Nat Nano* **5**, 190-194 (2010)
75. Vedala, H., Sorescu, D. C., Kotchey, G. P. and Star, A. Chemical Sensitivity of Graphene Edges Decorated with Metal Nanoparticles. *Nano Letters* **11**, 2342-2347 (2011)